



1 **Cyclic activity of Fuego de Colima volcano (Mexico):**
2 **insights from satellite thermal data and non-linear models**

3
4 Silvia Massaro^{1*}, Antonio Costa², Roberto Sulpizio^{1,3}, Diego Coppola⁴, Lucia Capra⁵

5
6 ¹Istituto per la Dinamica dei Processi Ambientali – Consiglio Nazionale delle Ricerche, Via R. Cozzi 53, 20125, Milan (Italy)

7 ²Istituto Nazionale di Geofisica e Vulcanologia, Via D. Creti 12, 40128, Bologna (Italy)

8 ³Dipartimento di Scienze della Terra e Geoambientali, Università di Bari, Via Orabona 4, 70125, Bari (Italy)

9 ⁴Dipartimento di Scienze della Terra, Università di Torino, Via Valperga Caluso, 35, 10129, Turin (Italy)

10 ⁵Centro de Geociencias UNAM, Campus Juriquilla, Queretaro (Mexico)

11
12 *Corresponding Author: Silvia Massaro (silvia-massaro@libero.it)

13
14
15 **Abstract**

16
17 The Fuego de Colima volcano (Mexico) showed a complex eruptive behaviour with periods of
18 rapid and slow lava dome growth, punctuated by explosive activity. We reconstructed the weekly
19 discharge rate average between 1998 and 2018 by means of satellite thermal data integrated with
20 published discharge rate data. By using spectral and wavelet analysis, we found a multi-year long-,
21 multi-month intermediate-, and multi-week short-term cyclic behaviour during the period of the
22 investigated eruptive activity, as those of many others dome-forming volcanoes. We use numerical
23 modelling in order to investigate the non-linear cyclic eruptive behaviour considering a magma
24 feeding system composed of a dual or a single magma chamber connected to the surface through an
25 elastic dyke evolving into a cylinder conduit in the shallowest part. We investigated the cases in
26 which the periodicity is controlled by i) the coupled deep-shallow magma reservoirs, ii) the single
27 shallow chamber, and iii) the elastic shallow dyke when is fed by a fixed influx rate or a constant
28 pressure. The model outputs indicate that the observed multi-year periodicity (1.5-2.5 years) can be
29 described by the fluctuations controlled by a shallow magma chamber with a volume of 20-50 km³
30 coupled with a deep reservoir of 500 km³, connected through a deep elastic dyke. The multi-month
31 periodicity (ca. 5 - 10 months) appears to be controlled by the shallow magma chamber for the
32 same range of volumes. The short-term multi-week periodicity (ca. 2.5 - 5 weeks) can be
33 reproduced considering a fixed influx rate or constant pressure at the base of the shallower dyke.
34 This work provides new insights on the non-linear cyclic behaviour of Fuego de Colima, and a
35 general framework for the comprehension of eruptive behaviour of andesitic volcanoes.



36 1. Introduction

37 Lava dome forming eruptions are relatively long-lived events, lasting from several months to
38 several decades (e.g. Merapi, Indonesia, Siswowardjojo et al., 1995; Kelut, Indonesia, De Bézizal et
39 al., 2012; Fuego de Colima, Mexico, Lamb et al., 2014; Santiaguito, Guatemala, Harris et al.,
40 2002), and usually punctuated by dome collapses and explosive (Vulcanian) episodes. Discharge
41 rates can change widely over a range of time scales, reflecting the physical mechanisms involved in
42 the transfer of magma to the Earth's surface (Melnik et al., 2008; Odbert and Wadge 2009). Dome
43 growth is not a continuous process and periodic behaviour has been commonly observed at several
44 volcanoes, including Santiaguito (Guatemala, Harris et al., 2003), Mt St Helens (USA, Swanson
45 and Holcomb, 1990), and Soufrière Hills (Montserrat, Voight et al., 1998; Loughlin et al., 2010;
46 Wadge et al., 2010; Nicholson et al., 2011). Periodic behaviours can be complex, showing
47 systematic or non-systematic temporal changes as the eruption progresses (Denlinger and Hoblitt,
48 1999; Costa et al., 2007a; Melnik et al., 2008; Bernstein et al., 2013; Wolpert et al., 2016), and may
49 be characterized by short-, intermediate- and long-term periodicities (Costa et al., 2007a; Melnik et
50 al., 2008; Costa et al., 2012; 2013; Melnik and Costa, 2014). The short- and intermediate-term
51 periodicities (hours or weeks) are generally explained by the upper conduit pressurization related to
52 the non-linear ascent of magma flow (Denlinger and Hoblitt, 1999; Melnik and Sparks, 1999;
53 Voight et al., 1999; Wylie et al., 1999; Ozerov et al., 2003; Lensky et al., 2004, Costa et al.,
54 2007a,b; 2012; Kozono and Koyaguchi, 2012). This is because the lower part of the dyke-conduit
55 acts as a capacitor that allows magma to be stored temporarily and released during the more intense
56 phase of discharge (Costa et al., 2007a,b; Melnik et al., 2008; Costa et al. 2012; 2013). The long-
57 term periodicity, with time scales from months to decades (Voight et al., 2000; Belousov et al.,
58 2002; Sparks and Young, 2002; Wadge et al., 2006), is usually controlled by pressure variations in
59 magma reservoirs (Barmin et al., 2002; Costa et al., 2007b; Melnik et al., 2008; Melnik and Costa,
60 2014). Since historical times, the Fuego de Colima volcano (Mexico; Fig.1a) has been characterised
61 by decade-lasting cycles of dome growth alternating with Vulcanian explosions, ended with sub-



62 Plinian eruptions (the last two occurred in 1818 and 1913, (Luhr, 2002; Saucedo et al., 2005; Norini
63 et al., 2010; Heap et al., 2014; Massaro et al., 2018a). The most recent cycle started after the 1913
64 eruption, and it is characterized by lava domes extruded with minor seismicity at high magma
65 temperatures (960-1020°C; Savov et al., 2008). As for other dome eruptions (Sparks, 1997), dome
66 growth at Fuego de Colima can be explained by complex non-linear pressure variations during
67 magma ascent from magma reservoirs (e.g. Melnik and Costa, 2014), cooling, crystallization,
68 degassing (e.g. Melnik and Sparks, 1999; Lensky et al., 2004; Nakanishi and Koyaguchi, 2008;
69 Kozono and Koyaguchi, 2012) and upper conduit geometric configurations characterized by
70 multiple pathways (e.g. Lavallée et al., 2012; Reubi et al., 2015).

71 Two magma chambers located at different depths characterize the feeding system of Fuego de
72 Colima volcano (Fig. 1b), with roofs located at ca. 6 (shallow magma chamber) and ca. 15 km
73 (deep magma chamber) of depth, as indicated by petrographic studies (Macias et al., 2017) and
74 geophysical data (Spica et al., 2017).

75 The purpose of this study is to investigate the existence of pattern of oscillations in discharge rates
76 during the 1998-2018 erupted activity at Fuego de Colima volcano. The available geological,
77 geophysical, and petrological data for this recent activity provide a remarkable opportunity to
78 improve the characterization and our understanding about the physical processes underlying cyclic
79 extrusion of lava domes. In particular, we used thermal remote sensing data along with published
80 effusion rates for reconstructing the oscillatory magma discharge rate behaviour of effusive activity
81 at Colima.

82 The availability of satellite thermal images in the last decade has strengthened the use of thermal
83 data for observing volcanic activity (e.g. Ramsey and Harris, 2012), especially in studying the
84 relationships with lava discharge rates (Coppola et al., 2009; Harris et al., 2010; Garel et al., 2012).
85 Coppola et al. (2013) propose that the radiant density of effusive/extrusive activity can be used to
86 estimate lava discharge rates and erupted volumes by means of empirical relationship based on SiO₂
87 content of the erupted lava. Although it is still under debate, the so-called “thermal approach”



88 (Dragoni and Tallarico, 2009) offers a good way for monitoring volcanic activity, especially when
89 direct observations are limited or absent.

90 Here we focus our attention to dynamics of fluctuations in magma discharge rate on various
91 timescales at Fuego de Colima volcano during 1998-2018. By using time series analytical
92 techniques (i.e. Fourier and wavelet analysis) we have identified three fundamental periodicities in
93 subsets of the time series: i) long-term (ca. 1.5-2.5 years), ii) intermediate-term (ca. 5-10 months),
94 iii) short-term (ca. 2.5-5 weeks), similar to those observed at many lava-dome eruptions (e.g. Costa
95 et al., 2012; Melnik and Costa, 2014; Christopher et al., 2015). These periodicities were compared
96 with numerical simulations provided by the model of Melnik and Sparks (2005) as generalized by
97 Costa et al. (2007a) for accounting the presence of a shallow dyke, and Melnik and Costa (2014) for
98 describing the control of a coupled dual chamber system. Numerical modelling of the different parts
99 of the plumbing system successfully reproduced the first-order cyclic behaviour of Fuego de
100 Colima during the 1998-2018 erupted activity. Our results highlighted that the dual magma
101 chamber dynamics controls the long-term periodicity evident during 2002-2006 and 2013-2016,
102 while the single magma chamber dynamics are more effective to explain the intermediate-term
103 periodicity in the same periods. Finally, the shallow dyke dynamics regulate the multi-week cycles
104 observed during 2002-2006 and 2011-2016.

105 The present work is divided in five main sections. The first describes the historical activity of the
106 Fuego de Colima, with particular attention to the recent period, from 1998 to 2018. The second
107 section describes the methods applied to the dataset composed of the satellite thermal data
108 integrated with published data. In particular, the Fourier analysis (including the discussion of its
109 limitations), the wavelet analysis with the definition of the wavelet transform, the choice of a
110 wavelet mother function, and the edge effects due to finite-length time series. It also includes the
111 use of the Melnik and Sparks (2014) model. The third section is dedicated to the input and target
112 data used for numerical simulations. The fourth presents the results obtained by the spectral and
113 wavelet analyses. This latter allows to establish significance levels for the wavelet power



114 spectrum. The periodicities observed in this spectrum were compared to the results obtained by
115 numerical simulations. The last fifth section contains a discussion on the eruptive behaviour
116 occurred at Fuego de Colima during 1998-2018, providing new insights from the observed data and
117 non-linear models.

118

119 **2. The historical activity of Fuego de Colima volcano**

120

121 Since historical times Fuego de Colima represents the most active volcano in Mexico, posing a
122 serious threat to all surrounding populations (Cortés et al., 2005; Gavilanes-Ruiz et al., 2009;
123 Bonasia et al., 2011). The earliest accounts of the volcano activity can be found in *Historia Antigua*
124 *de Mexico* (Clavijero, 1780), where the destructive effects of its explosive activity are carefully
125 described (Bretón-Gonzales et al., 2002). The historical activity of Fuego de Colima was described
126 and interpreted by several authors (Luhr and Carmichael, 1980; Medina-Martínez, 1983; De la
127 Cruz-Reyna, 1993; Bretón-Gonzales et al., 2002; Luhr, 2002). The Fuego de Colima has shown a
128 transitional eruptive behaviour spanning from effusive to explosive activity, dominated by dome
129 growth and Vulcanian eruptions. Occasionally sub-Plinian events occurred (1576, 1606, 1690, 1818
130 and 1913), indicating a recurrence time of approximately 100 years (De la Cruz-Reyna, 1993; Luhr,
131 2002; Saucedo et al., 2005; Gavilanes-Ruiz et al., 2009; Massaro et al. 2018a). The sub-Plinian
132 event occurred in 1913 (Saucedo et al., 2010) is the largest historical eruption and it has been used
133 as benchmark for volcanic hazard studies (Martin Del Pozzo et al., 1995; Saucedo et al., 2005;
134 Bonasia et al., 2011).

135

136 **2.1. The 1998-2018 eruptive activity**

137 The 1998-2018 is the only period of post 1913 activity for which there is sufficiently available
138 information to explore the cyclic activity of Fuego de Colima. Different periods of effusion (domes
139 and lava flows) punctuated by Vulcanian eruptions and dome collapses characterised the volcano



140 activity between 1998 and 2018 (Savov et al., 2008; Varley et al., 2010a; Hutchinson et al., 2013;
141 Mueller et al., 2013; Zobin et al., 2015; GVP, 2017). The duration of extrusive activity and magma
142 discharge rate varied through time, that was generally divided into five eruptive phases up to 2015;
143 I) 1998-1999; II) 2001-2003; III) 2004-2005; IV) 2007-2011; V) 2013-2015 (Zobin et al., 2015;
144 Arámbula-Mendoza et al., 2018).

145 The first dome extrusion started in November 1998, and quickly filled the 1994 explosion crater,
146 forming lava flows that descended the southern flanks of the Fuego de Colima cone during most of
147 1999 ($> 5 \text{ m}^3 \text{ s}^{-1}$) in average for Mueller et al., 2013; $4.11 \text{ m}^3 \text{ s}^{-1}$) in average for Reubi et al.,
148 2013).

149 At the beginning, this dome grew rapidly (ca. $4.4 \text{ m}^3 \text{ s}^{-1}$) reaching a volume of ca. $3.8 \times 10^5 \text{ m}^3$ in
150 24 hours. During this period the effusion rate reached a peak value around $30 \text{ m}^3 \text{ s}^{-1}$ (Navarro-
151 Ochoa et al., 2002; Zobin et al., 2005; Reubi et al., 2015) and showed a cyclic damped behaviour
152 soon after. During 1999-2001 a series of explosions destroyed the dome and excavated a large
153 apical crater (Bretón-Gonzales et al., 2002).

154 A slow outpouring of lava ($< 1 \text{ m}^3 \text{ s}^{-1}$) for Mueller et al., 2013; $0.17 \text{ m}^3 \text{ s}^{-1}$) for Reubi et al., 2013;
155 2015) resumed in May 2001 and continued for 22 months. In February 2002, the lava dome
156 overflowed the crater rims producing lava flows. During this eruptive phase, the magma extruded
157 from three separate vents with only minor explosive activity, at a rate of ca. $0.9 \text{ m}^3 \text{ s}^{-1}$ (GVP,
158 2002). Vulcanian explosions dismantled the dome during July and August 2003 (GVP, 2003).

159 In September 2004, low-frequency seismic swarms heralded the onset of the new effusive phase
160 (Varley et al., 2010a; Arámbula-Mendoza et al., 2011; Lavallée et al., 2012) with a small increase
161 in average discharge rate of $0.6 \text{ m}^3 \text{ s}^{-1}$ (Reubi et al., 2013; 2015). The lava dome building occurred
162 from the end of September until the beginning of November, with a magma effusion rate up to 7.5
163 ($\text{m}^3 \text{ s}^{-1}$) in October (Zobin et al., 2008; 2015). The effusive activity was accompanied and followed
164 by intermittent Vulcanian explosions. The explosive activity diminished in intensity during
165 December 2004-January 2005. From February to September 2005, effusion and large explosions



166 occurred.

167 In the following months, small, short-lived domes were observed, with an estimated effusion rate
168 between 1.2 – 4.6 ($\text{m}^3 \text{s}^{-1}$) (Varley et al., 2010b; Reubi et al., 2015). In May and June, the explosive
169 activity produced pyroclastic density currents reaching distances up to 5.4 km from the volcano
170 summit (Varley et al., 2010a).

171 In February 2007, a new lava dome began to grow and explosions were reported in the period
172 between January 2009 and March 2011. The 2007-2011 period of dome extrusion represents the
173 slowest growth rate in the recent history of Fuego de Colima. Hutchinson et al. (2013) calculated a
174 mean effusion rate of ca. 0.02 ($\text{m}^3 \text{s}^{-1}$) from 2007 to 2010 using digital photographic data, in good
175 accordance with Zobin et al. (2015) that reported extrusion rates of 0.03 ($\text{m}^3 \text{s}^{-1}$) during 2007.
176 Mueller et al. (2013) estimated the magma extrusion rate between 0.008 ± 0.003 ($\text{m}^3 \text{s}^{-1}$) to $0.02 \pm$
177 0.007 ($\text{m}^3 \text{s}^{-1}$) during 2010, which dropped down to 0.008 ± 0.003 ($\text{m}^3 \text{s}^{-1}$) again in March 2011. On
178 21 June 2011 an explosion heralded the cessation of dome growth and marked the end of the
179 effusive period.

180 After 1.5 years of rest, in January 2013 a sequence of explosions cored out the 2011 dome and
181 generated pyroclastic density currents that reached distances of up to 2.8 km from the summit
182 (GVP, 2013). From March to October, the calculated discharge rate was in the range of 0.1 – 0.2
183 ($\text{m}^3 \text{s}^{-1}$) (Reyes-Dávila et al., 2016). Successively, the mid-low explosive activity took place up to
184 February-March 2014, until a new pulse of magma observed in July, with an approximate rate of 1-
185 2 ($\text{m}^3 \text{s}^{-1}$) (Arámbula-Mendoza et al., 2018). On January 11, 2015, a new lava dome was observed
186 inside the crater (Thiele et al., 2013) and its growth continued until July, with effusion rate of ca.
187 0.27 ($\text{m}^3 \text{s}^{-1}$) (Zobin et al., 2015). Between 10-11 July 2015 the recent dome was destroyed by the
188 most intense activity since the 1913 eruption (Capra et al., 2016; Reyes-Dávila et al., 2016). In the
189 2013-2015 period, the average extrusion rate was of ca. 0.2 ($\text{m}^3 \text{s}^{-1}$) (Thiele et al., 2017), with peak
190 values > 10 ($\text{m}^3 \text{s}^{-1}$) (Varley, 2015). After that, the eruptive activity ceased until January 2016 when
191 daily ash plumes started to occur along with active lava flows and explosions. In early July a new



192 dome began to grow, overtopping the crater rim. A large explosion was recorded on 10 July 2016,
193 followed by daily and multiple-daily ash plumes up to the end of year. Multiple flows descended
194 from lava dome during September-December. In 2017 frequent strong explosions and ash emissions
195 were recorded until March. Through June decreasing seismicity and minor landslides were reported
196 with no evidence of effusive activity or new dome growth (GVP, 2017). Here we provide a more
197 systematic overview of the 1998-2018 erupted activity, obtained by satellite thermal data along with
198 some published data, explained in the following section.

199

200 3. Methods

201 We analysed the thermal energy spectrum of Fuego de Colima volcano available from March 2000
202 to October 2018, detected Middle Infrared Observation of Volcanic activity (MIROVA) hot-spot
203 detection system (Coppola et al., 2016). The period 1998-1999 was integrated using published
204 discharge rates (Navarro-Ochoa et al., 2002; Zobin et al., 2005). The MIROVA NRT system is
205 based on the near real time (NRT) analysis of the MODerate resolution Imaging Spectroradiometer
206 (MODIS) data, distributed by the LANCE-MODIS data system (<http://modis.gsfc.nasa.gov/>).

207 The thermal emission from an object is attenuated by the atmosphere resulting from absorption by
208 gases and scattering by particles. MIROVA system focuses on the Middle InfraRed region (MIR),
209 which shows the lowest attenuation levels, to better detect and analyse thermal radiation emitted
210 from volcanic sources. While the standard MODIS forward processing delivers Aqua and Terra
211 images within 7-8 hours of real time, LANCE-MODIS allows for the creation of MIROVA radiant
212 flux timeseries within 1-4 hours from the satellite overpass (www.mirovaweb.it). This thermal data
213 collection was converted into lava discharge rate estimates and integrated with some published data
214 in order to reconstruct the weekly mean discharge rate spectrum from 1998 to 2018 (Fig. 2a).

215 In this work, we refer to Coppola et al. (2013), who describes the relationship between the heat lost
216 by lava thermal radiance variations and discharge rates, by means of a unique, empirical parameter.



217 They compared the energy radiated during several distinct eruptions to the erupted lava volumes
218 (m^3). The relationship between the Volcanic Radiated Energy (VRE) and the erupted volume was
219 defined by introducing the concept of radiant density (c_{rad} , in J m^{-3}). This parameter is analysed as a
220 function of the SiO_2 content and the bulk rheological properties of the related lava bodies. It is
221 strongly controlled by the characteristic thickness of the active lavas at the time of a satellite
222 overpass, whereas the effects of variable degree of insulation, morphology and topographic
223 conditions produce only a limited range of variability ($\pm 50\%$) (Coppola et al., 2013). For the Fuego
224 de Colima we used a value of $c_{rad} = 3.90 \times 10^7 (\text{J m}^{-3})$ with a SiO_2 content of 59.6% (Savov et al.,
225 2008; Coppola et al., 2013). We obtained the cumulative volumes of effusion per year (from 2000
226 to 2018) considering the ratio between the average VRE estimations and c_{rad} . It is important to stress
227 that the instrumental limit of the MIROVA system is not able to detect thermal anomalies below
228 0.5–1 MW. Since we used a radiant density (c_{rad}) of $3.90 \times 10^7 (\text{J m}^{-3})$, the minimum reliable value
229 of discharge rate is $0.01 (\text{m}^3 \text{ s}^{-1})$ (Coppola et al., 2013). As reported by Coppola et al. (2016), the
230 thermal data obtained from MIROVA are not correct due to the presence/attenuation of clouds. For
231 this reason, the estimates of effusion rates and volumes are to be considered as minimum estimates.

232 Because the 2002-2006 and 2013-2016 intervals are the most active in the analysed period, we
233 firstly applied the Fourier analysis to the monthly average of discharge rates (Fig. 2b) of these time
234 intervals, in order to explore the modal spectrum of the signal. Although Fourier analysis is well
235 suited to the quantification of constant periodic components in a time series, it cannot recognise
236 signals with time-variant frequency content. Whereas a Fourier Transform analysis may determine
237 all the spectral components embedded in a signal, it does not provide any information about timing
238 of occurrence. To overcome this problem, several solutions have been developed in the past
239 decades that are able to represent a signal in the time and frequency domain at the same time.

240 The aim of these approaches is to expand a signal into different waveforms with local time–
241 frequency properties well adapted to the signal structure (Cazellas et al., 2008). In order to get



242 information on the amplitude of the periodic signals within the Fuego de Colima (MIROVA) time
 243 series, we performed a wavelet analysis by decomposing the weekly time series (Fig. 2a) into
 244 time/frequency space (Fig. 3).

245 Wavelet analysis is a powerful tool largely used in many scientific fields (i.e., ecology, biology,
 246 climatology, geophysics) and engineering. It is especially relevant to the analysis of non-stationary
 247 systems (i.e., systems with short-lived transient components, Cazellas et al., 2008). For this study,
 248 practical details in applying wavelet analysis were taken from Torrence and Compo (1998) and
 249 Odbert and Wadge (2009). It is worth noting that wavelet analysis considers a wave that decays
 250 over a finite time and whose integral over infinite time is zero. Many forms of wavelet (called
 251 “wavelet functions” $\psi(\eta)$, or “mother functions”, which depend on a non-dimensional time
 252 parameter “ η ”) have been designed for analytical use (Farge, 1992; Weng and Lau, 1994;
 253 Daubechies, 1994), each with its own characteristics that make it suitable for certain applications.
 254 The choice of the wavelet can influence the time and the scale resolution of the signal
 255 decomposition. Wavelet analysis is popular in geosciences (Trauth, 2006), as it does not require
 256 any a priori understanding of the system generating the time series.

257 Our time series (weekly average discharge rates acquired mainly by the MIROVA system; Fig. 2a),
 258 called (x_n) , has equal time spacing ($\delta t = 7$ days) and number of points $n = 0 \dots N-1$. Using the
 259 approximately orthogonal Morlet function as wavelet function $\psi(\eta)$ (it must have zero mean and
 260 be localized in both time and frequency space; Farge, 1992), we here define the wavelet transform
 261 $W_n(s)$ as the convolution of x_n with a scale (s) and translated version of $\psi_0(\eta)$ (mother function). In
 262 formula:

$$263 \quad W_n(s) = \sum_{n'=0}^{N-1} x_{n'} \psi^* \left[\frac{(n' - n)\delta t}{s} \right] \quad (1)$$

264 where the (*) indicates the complex conjugate. The scale s should be equal to approximately $2\delta t$,



265 according to the Nyquist theorem. Therefore, the smallest wavelet we could possibly resolve is $2\delta t$,
266 thus we choose $s_0 = 14$ days. Generally, $\psi(\eta)$ is a complex function, therefore the wavelet transform
267 is also complex. It is possible to reconstruct the “local” wavelet power spectrum as the absolute-
268 value squared of the wavelet coefficients, $|Wn(s)|^2$. The way to compute the wavelet transform for a
269 time series is to find the Fourier transform of both the wavelet function (Morlet in our case) and the
270 time series. Following Torrence and Compo (1998), we made the normalization by dividing by the
271 square-root of the total wavelet variance (σ^2).

272 Usually, a periodic component in a time series may be identified in a power spectrum if it has
273 distinctly greater power than a mean background level (that would correspond to a Gaussian
274 background noise) (Odbert and Wadge, 2009). However, the spectra generated from many
275 geophysical systems indicate that the noise in time series data tends not to have a Gaussian
276 distribution (Vila et al., 2006) but it can be better described by coloured noise, specifically red noise
277 (Fougere, 1985). For this reason we use a simple model for red noise given by the univariate lag-1
278 autoregressive or Markov process (Torrence and Compo, 1998) in order to determine the
279 significance levels for our wavelet spectrum. These background spectra are used to establish a null
280 hypothesis for the significance of a peak in the wavelet power spectrum. The null hypothesis is
281 defined for the wavelet power spectrum considering that the time series has a mean power
282 spectrum: if a peak in the wavelet power spectrum is significantly above this background spectrum,
283 then it can be assumed to be a true feature with a certain percentage of confidence. For definitions,
284 “significant at the 5% level” is equivalent to “the 95% confidence level” (Torrence and Compo,
285 1998). The confidence interval is defined as the probability that the true wavelet power at a certain
286 time and scale lies within a certain interval about the estimated wavelet power (Torrence and
287 Compo, 1998). Because we deal with finite-length time series, errors occur at the beginning and end
288 of the wavelet power spectrum. A solution is to pad the end of the time series with zeroes to bring
289 the total length N up to the next-higher power of two, thus limiting the edge effects. However,



290 padding with zeroes introduces discontinuities at the endpoints and, especially towards larger
291 scales, decreasing the amplitude near the edges as more zeroes enter the analysis (Torrence and
292 Compo, 1998). The cone of influence (COI) is the region of the wavelet spectrum in which edge
293 effects become important. The criterion for applying wavelet analysis is very similar to those
294 employed with classic spectral methods. In other words, the wavelet transform can be regarded as a
295 generalization of the Fourier transform, and by analogy with spectral approaches, we compute the
296 local wavelet power spectrum as described above. Successively, this can be compared with the
297 “global” wavelet power spectrum which is defined as the averaged variance contained in all wavelet
298 coefficients of the same frequency (Torrence and Compo, 1998; Cazellas et al., 2008).

299 Numerical simulations have been carried out using the magma flow model of Melnik and Costa
300 (2014), who generalized the model proposed by Melnik and Sparks (2005) for a magma chamber
301 connected to a dyke that evolves into a cylindrical conduit near surface. In particular, the model of
302 Melnik and Costa (2014) accounts for the possibility of a dual magma chamber system. The model
303 accounts for rheological changes due to volatile loss and temperature driven crystallization. These
304 processes are both effective during dome extrusion eruptions because of the typical low magma
305 ascent velocities (from millimetres to few centimetres per second), which can result in magma
306 transit times from days to weeks. These ascent times are often comparable with those of crystal
307 nucleation and growth, allowing efficient heat exchange between magma and wall rocks (Melnik
308 and Sparks, 1999; 2005; Costa et al., 2007c).

309

310 **4. Input and target data for numerical simulations**

311 4.1 Geometrical configurations of the magma plumbing system

312

313 The physical framework used in the Melnik and Costa (2014) the model (Fig. 1b) consists of two
314 magma chambers located at different depths, with chamber pressures P_{chs} and P_{chd} able to drive the



315 magma ascent in an elliptical cross-section volcanic conduit (approximating a dyke). Near surface
316 the conduit evolves into a cylinder at depth L_T (named “transition level”).

317 Numerical simulations were carried out considering the shallower magma chamber (single magma
318 chamber configuration) or the double magma chamber. The single magma chamber model
319 considers a conduit feeding system composed of a shallow dyke (d_s) that connects the magma
320 chamber to a shallower cylinder, in agreement with geological and geophysical evidence from
321 different volcanoes (Melnik and Sparks, 2005; Costa et al., 2007a; Melnik et al., 2008; Melnik and
322 Costa, 2014). The double magma chamber model includes the addition of a deep reservoir
323 connected to the shallow chamber through an elastic deep dyke (d_d) (Fig. 1b).

324 In order to reproduce the observed fluctuations in discharge rates recorded in some periods of the
325 1998-2018 erupted activity, we considered a discharge rate regime where the period of pulsations is
326 controlled by the elasticity of the shallow dyke, and a discharge rate regime where the periodicity is
327 controlled by the volume of the single or dual magma chamber(s) (Barmin et al., 2002; Melnik and
328 Sparks, 2005; Costa et al., 2007a; Melnik and Costa, 2014).

329 In Appendices A2 and A3 we reported some test simulations in order to show the control of the
330 most sensitive parameters (i.e. water content in magma, dyke dimensions, volume of magma
331 chamber, magma influx rate into the magma chamber) affecting the model outputs in case of the
332 single magma chamber model. The volumes of the magma chamber (V_{ch}) range from 20 to 50 km³
333 and the width of the feeder dyke $2a$ from 200 to 400 m (Massaro et al., 2018a).

334 In Appendix A4 is shown the sensitivity test aimed to explore a broad range of chamber volumes
335 and aspect ratios in the case of double magma chamber configuration. The deep chamber has its top
336 at 15 km of depth, it is pressurised and fed from below by a constant influx $Q_{in,d}$. The volumes of
337 shallow magma chamber (V_{chs}) range from 30 to 50 km³, and from 550 to 750 km³ for the deep
338 magma chamber (V_{chd}), according to geophysical data (Cabrera-Espindola, 2010; Spica et al.,
339 2017). The aspect ratios for shallow and deep magma chambers ($AR_s - AR_d$) varied from 1 to 2. For
340 each run included in the sections 1-3 of A4, we used a fixed influx $Q_{in,d} = 2.3$ (m³ s⁻¹), and variable



341 widths of the deeper dyke ($2a_{od}$) from 200 to 3000 m. The lower dyke thickness $2b_{od}$ is not an input
 342 data of the model as it changes as function of local pressure conditions, therefore it does not appear
 343 in the diagrams. In Section 4 of A4 we show two sets of runs having $Q_{in,d}$ equal to 1 and 3 ($\text{m}^3 \text{s}^{-1}$)
 344 respectively, and the following fixed parameters: AR_s and $AR_d = 1$, $V_{chd} = 650 \text{ km}^3$, $V_{chs} = 40 \text{ km}^3$.

345

346 4.2 Petrological data

347

348 Erupted products at Fuego de Colima are chemically intermediate and primarily andesitic lavas with
 349 ca. 61 wt.% SiO_2 , (Lavallè et al., 2012). The observed dome growth phases are usually fed by
 350 prolonged magma ascent times, which allow efficient degassing and crystallization. This is in
 351 agreement with the low mean porosity (14-16% e.g Lavallè et al., 2012; Farquharson et al., 2015)
 352 and low water contents of the products of the recent activity (2 wt. % for 1998-1999, Mora et al.,
 353 2002; 0.1-2.5 wt. % for 1998-2005 products, Reubi and Blundy, 2008). Dome lava currently
 354 erupted exhibits a range of crystallinities (phenocrysts, 20–30 vol.%; microlites, 25–50 vol.%), and
 355 the groundmass constitutes as much as 68 vol.% (Luhr, 2002). The andesites show a porphyritic
 356 texture with plagioclase (13–25 vol.%), orthopyroxene (2– 4 vol.%), clinopyroxene (3–4 vol.%) and
 357 minor hornblende (<0.5%) and Fe–Ti oxides (ca. 2 vol.%). Olivine occurs rarely as xenocrysts
 358 (Lavallè et al., 2012). According to Costa et al (2007a), magma viscosity increases due to the
 359 crystal fraction β as described through the function $\Theta(\beta)$ (Costa et al., 2009):

$$360 \quad \theta = \frac{1 + \left(\frac{\beta}{\beta^*}\right)^\delta}{\left(1 - \text{erf}\left(\frac{\sqrt{\pi}}{2\varepsilon} \frac{\beta}{\beta^*} \left[1 + \left(\frac{\beta}{\beta^*}\right)^\gamma\right]\right)\right)^{2.5\beta^*}} \quad (2)$$

361 where β^* represents the critical transition fraction, γ is a measure of the steepness of the rheological
 362 transition, ε ($0 < \varepsilon < 1$) determines the value of $\Theta(\beta^*)$. In principle β , γ , δ and ε can be described a
 363 function of the strain rate and crystal shape but here are assumed to be constant (Costa et al.,
 364 2007a). As crystallization proceeds the remaining melt becomes more silica rich and viscosity



365 increases (Costa et al., 2007a). Table 1 summarises the value ranges used for the input parameters
366 of the model.

367

368 5. Results

369 In Figure 2 we showed the averages of discharge rates at Fuego de Colima volcano from November
370 1999 to October 2018. Here we define as “high” discharge rates values $> 0.1 \text{ (m}^3 \text{ s}^{-1}\text{)}$ (highlighted as
371 dark blue areas). All values below $> 0.1 \text{ (m}^3 \text{ s}^{-1}\text{)}$ are considered “low” discharge rates (light blue
372 areas). Volcanological observations are reported at the top and the bottom of the diagram. In
373 addition, we distinguished between lava flows and lava domes accordingly to the dominant
374 emplacement style typical of each eruption, and between “low” (i.e. ash plumes, gas emissions) and
375 “high” (i.e. strong explosions, Vulcanian eruptions) magnitude explosive activity.

376 The weekly average of discharge rates represents the complete dataset used in this study, and is
377 reported in Figure 2a. These data have been calculated by using the MIROVA data (black dots) for
378 the 2000-2018 period, and complemented with published data (blue crosses) for the 1998-1999
379 period (Navarro-Ochoa et al., 2002; Zobin et al., 2005). Even if the data detection of satellite
380 thermal energy represents a continuous spectrum of information, it is worth noting that it suffers of
381 some limitations connected to cloud covering, magma composition, rheology, and emplacement of
382 the investigated lava body due to topographic conditions (Harris and Rowland, 2009; Harris et al.,
383 2010; Coppola et al., 2013).

384 Figure 2b shows the monthly discharge rate spectrum from 1998 to 2018 using the MIROVA
385 dataset (black dots), integrated with available published data (blue crosses) (Navarro-Ochoa et al.,
386 2002; Zobin et al., 2005; Capra et al., 2010; Varley et al., 2010a; Sulpizio et al., 2010; James and
387 Varley, 2012; Hutchinson et al., 2013; Reubi et al., 2013; Varley, 2015; Reyes-Dávila et al., 2016;
388 Thiele et al., 2017; GVP, 2000; 2017). Figure 2c summarizes the yearly average of discharge rates



389 from MIROVA dataset, highlighting the good agreement with the available average estimation of
390 yearly discharge rates from literature (Mueller et al., 2013; Reyes-Dávila et al., 2016; Aràmbula et
391 al., 2018; GVP, 1998-2017).

392

393 5.1 Fourier analysis

394 The Fourier analysis applied to 2002-2006 period showed two periodic components, $T_0 = 24.70$ and
395 $T_1 = 6.17$ corresponding to ca. 2 years and ca. 6 months, respectively (Appendix A1, Fig. a). For
396 2013-2016 we obtained similar results: $T_0 = 24.94$ and $T_1 = 6.23$ corresponding to ca. 2.1 years and
397 ca. 6 months, respectively (Appendix A1, Fig. b).

398

399 5.2 Morlet wavelet analysis

400 The wavelet analysis is well suited for investigations of the temporal evolution of aperiodic and
401 transient signals. Indeed, wavelet analysis is the time–frequency decomposition with the optimal
402 trade-off between time and frequency resolution (Lau and Weng, 1995; Mallat, 1998). The whole
403 analysed dataset is composed of 825 data points, representing the time evolution of the oscillating
404 components of the 1998-2018 eruptive activity (Fig. 2a). Figure 3a shows the normalised local
405 wavelet power spectrum of the signal. The colours scale for power values vary from light orange
406 (low values) to dark red (high values). The thick black contours represent the 95% confidence level.
407 The blue line indicates the cone of influence (COI) that delimits the region not influenced by edge
408 effects. From this analysis, it is easy to observe three main periodicities during 2002-2006 and
409 2013-2016 periods: i) long-term periodicity of ca. 1.5–2.5 years; ii) intermediate-term periodicity of
410 ca. 5-10 months; and, iii) short-term periodicity of ca. 2.5-5 weeks. The short-term periodicity is
411 also present in 2011 (Fig. 3a). Figure 3b shows the global wavelet spectrum corresponding to the
412 local wavelet power spectrum plotted in Fig. 3a. The green dashed line shows the position of the
413 best-fitting red noise model at the 95% confidence level.



414 5.3 Numerical simulations

415 Appendices A2-A4 provide some sensitivity tests in order to explore the effects of different
416 parameters on discharge rate fluctuations for the single (A2-A3) and dual magma chamber model
417 (A4). In particular, in Appendix A2 is reported the general steady-state solution of the numerical
418 model, with both stable and unstable branches (e.g. Melnik et al., 2008; Nakanishi and Koyaguchi,
419 2008), showing that the cyclic behaviour can occur only between 2 and 4 ($\text{m}^3 \text{s}^{-1}$), for the fixed
420 input data (panel (a)). Varying the width of the shallow dyke $2a$ (from 200 to 400 m) and water
421 content in the melt phase, we observed how the unstable branch changes its shape. This implies
422 different periods of possible oscillations in discharge rate (panels (b)-(c)).

423 Appendix A3 provides a set of simulations carried out varying the width of the shallow dyke $2a$
424 (panel (a)). The resulting periodicities vary from ca. 1000 days ($2a = 200$ m) ca. 500 days ($2a = 300$
425 m) to ca. 250 days ($2a = 400$ m). These results highlight negative correlation between dyke widths
426 and periods of oscillation (Costa et al., 2007a). In this case, the variable widths influence the
427 intensity and periodicity of discharge rates: the wider the dyke, the lower the intensity and
428 periodicity of discharge rates. Differences in the amplitude of oscillations are observed in panel (b),
429 highlighting a positive correlation between the volume of the magma chamber V_{ch} and periodicities.
430 Periodicities of ca. 500 days correspond to 20 - 30 km^3 , while larger values of ca. 970 and ca. 1176
431 days are provided for 40 and 50 km^3 , respectively.

432 In panel (c), we reported also a set of simulations considering the modelled discharge rate
433 controlled by the elasticity of the shallower dyke with fixed influx rates Q_{in} (in the range of 0.01 -
434 0.1 $\text{m}^3 \text{s}^{-1}$). Although this set of runs showed damped oscillations, which do not represent the
435 periodicities observed at Fuego de Colima, it shed lights on the model's output variability in
436 relation to the boundary conditions.

437 Appendix A4 contains the sensitivity tests for the dual magma chamber model. As reported in
438 Melnik and Costa (2014), the dual chamber model shows cyclic behaviour with a period that



439 depends on the intensity of the influx rate and the chamber connectivity (described as the horizontal
440 extent of the dyke connecting the two chambers). For a weak connectivity, the overpressure in the
441 deeper chamber remains nearly constant during the cycle and the influx of fresh magma into the
442 shallow chamber is also nearly constant. For a strong connectivity between the two chambers, their
443 overpressures increase or decrease during the cycle in a synchronous way. Influx into the shallow
444 chamber stays close to the extrusion rate at the surface (Melnik and Costa, 2014). We explored
445 different cases considering various fixed parameters as follow: *i*) volumes of the shallow and deep
446 magma chambers ($V_{chs} = 40 \text{ km}^3$, $V_{chd} = 650 \text{ km}^3$); *ii*) aspect ratios ($AR_s = 1$, $AR_d = 1$) and the deep
447 magma chamber volume ($V_{chd} = 650 \text{ km}^3$); *iii*) aspect ratios ($AR_s = 1$, $AR_d = 1$) and the shallow
448 magma chamber volume ($V_{chs} = 40 \text{ km}^3$). For *i*), *ii*) and *iii*) cases, the deep influx rate $Q_{in,d}$ has fixed
449 values from 3 to 1 m^3/s . In conclusion, these sensitivity tests showed the passage from weakly
450 connected magma chambers (lack of simultaneous oscillation of $Q_{in,s}$ and Q_{out}) when $2a_{0d} = 200 \text{ m}$
451 to strongly connected magma chambers (synchronous oscillations of $Q_{in,s}$ and Q_{out}) when $2a_{0d} =$
452 3000 m.

453 Figure 4a shows a representative example of time-dependent solution for a discharge rate controlled
454 by the elasticity of the shallower dyke. Simulations were carried out using fixed values of pressure
455 (blue line) and influx rate ($Q_{in,s} = 3.5 \text{ m}^3/\text{s}$) (green line) at the source region of the shallower dyke.
456 The dyke is long 5500 m, it has width $2a = 400 \text{ m}$ and thickness $2b = 2 \text{ m}$ and a dyke-cylinder
457 transition at 1300 m of depth. The magma chamber volume is fixed to 30 km^3 . Solutions present
458 periodicities from 16 to 40 days in agreement with the weekly periodicities of ca. 38-18 days (ca.
459 2.5-5 weeks) derived from the wavelet analysis (Fig. 3a).

460 Figure 4b describes a representative example of the single magma chamber model simulations. We
461 set the magma feeding system composed of a dyke long 6500 m, having a width $2a = 600 \text{ m}$,
462 thickness $2b = 4 \text{ m}$, and a dyke-cylinder transition fixed at 1000 m of depth. The chamber has a
463 volume fixed to 30 km^3 and receives a constant $Q_{in,s} = 2.3 \text{ (m}^3 \text{ s}^{-1})$. The transient solution is
464 accounted for the discharge rate controlled by the magma chamber volume, showing an



465 intermediate-term periodicity of ca. 220 days, in agreement with the intermediate-term periodicity
466 of ca. 146-292 days (ca. 5-10 months) obtained from the wavelet analysis (Fig. 3a).

467 Figure 4c reports a representative example of the solution obtained with the dual magma chamber
468 model in order to assess the effect of the deep chamber on the discharge rate. We fixed the volumes
469 of deep and shallow magma chamber at 40 and 650 km³, respectively. The shallow dyke is 6500 m
470 long with a width $2a = 260$ m and thickness $2b = 4$ m. The deep dyke has a width $2a_{od} = 500$ m, and
471 a deep influx rate $Q_{in,d} = 2.3$ (m³ s⁻¹). A cyclic behaviour of ca. 825 days is observed, reaching a
472 peak discharge rate of ca. 6 (m³ s⁻¹). This result is in agreement with the long-term periodicity of ca.
473 547-913 days (ca. 1.5 - 2.5 years) derived from the wavelet analysis (Fig. 3a).

474

475 6. Discussions

476 In recent years, many studies have focused on magma flow dynamics in volcanic conduits during
477 lava dome building eruptions (Melnik and Sparks, 1999; Wylie et al., 1999; Barmin et al., 2002;
478 Melnik and Sparks, 2002; 2005; Costa et al., 2007a,b; Nakanishi and Koyaguchi, 2008; Kozono and
479 Koyaguchi, 2012), highlighting periodic variations in discharge rate due to the transition from low
480 regime (allowing efficient crystals grow leading to increase in magma viscosity) to high regime
481 (with negligible crystallization). This difference in discharge rates can be of orders of magnitude,
482 with strongly non-linear responses to the variation of governing parameters from the volcanic
483 system. This behaviour allows periodic oscillations of the discharge rate (Nakada et al., 1999; Watts
484 et al., 2002), as observed in different dome extrusion eruptions (e.g. Mt St. Helens, Santiaguito,
485 Montserrat, (Melnik et al., 2008). Although each volcano usually shows its complex pattern of
486 discharge fluctuations, the cause can be explained as the superimposition of long, intermediate, and
487 short-term effects of the coupled magma chamber(s) and conduit dynamics. The long-term
488 oscillations in discharge rate are function of magma chamber size, magma compressibility, and of
489 the amount and frequency of magma recharge and withdrawal (Barmin et al., 2002; Costa et al.,



490 2007b; Melnik et al., 2008; Costa et al., 2013; see Appendices A2-A3). The short-term and
491 intermediate oscillation dynamics can also superimpose to the main long-term periodicity, through
492 small changes in magma temperature, water content, and kinetic of crystallization during magma
493 transit in the conduit (e.g., Melnik et al., 2008). The aforementioned eruptive behaviour
494 characterized also the Fuego de Colima activity in the 1998-2018 period, as demonstrated by the
495 wavelet analysis of satellite thermal data. It is worth noting that the oscillating behaviour is not
496 regular, having a period, between 2007 and 2012, that does not show any significant periodicity
497 (Fig. 3a). During this period the volcano enter in an almost quiescent status with very low discharge
498 rates. This period of low discharge rates is punctuated by low explosive activity, triggered by dome
499 collapse or pressurization of the upper conduit.

500 In order to investigate the relationship between the periodic components observed in wavelet
501 analysis and the dynamics of the Fuego de Colima feeding system, we run simulations using the
502 numerical model Melnik and Costa (2014) (Fig. 4). The model can reproduce the results of the
503 wavelet analysis in terms of observed periodicities, allows us to relate short-, intermediate- and
504 long-term oscillations in discharge rates to the dynamics of upper conduit, shallow magma
505 chamber, and coupled shallow and deep magma chambers, respectively. This implies that the
506 pressurization of the deep magma chamber has cascade effects on the whole feeding system of the
507 Fuego the Colima, similarly to what observed in other recent lava dome eruptions (i.e. Montserrat;
508 (Melnik and Costa, 2014). It is of particular interest that the best output with the dual magma
509 chamber model indicates that chambers do not oscillate simultaneously (“decoupled oscillation”;
510 Fig. 4c). This accounts for the coexistence of long and intermediate periodicities in the 2002-2006
511 and 2013-2016, which would have not been possible in case of synchronous oscillation of the two
512 magma chambers. It means that the influx of magma from the deeper into the upper feeding system
513 induces pressurization to the shallow system (magma chamber + conduit), which starts to oscillate
514 following its own periodicities.

515 Although the presented data provide, for the first time, a framework able to explain the periodic



516 behaviour of effusive activity at Fuego de Colima volcano, both numerical model and wavelet
517 analysis suffer of some limitations that need to be taken into account in interpreting the results:

518 *i)* the available data of discharge rates and dome volumes collected for the 1998-2018
519 period do not have the same quality. For this reason, this lead us to extract only averages of
520 discharge rate for the entire period, with biasing effects to lower amplitudes;

521 *ii)* a common weakness of the spectral and wavelet analysis techniques is their inability to
522 distinguish the source of any given periodic component (i.e. whether it is a signal from a
523 volcanic process, an external process or if it is noise in the data). Elucidating the exact
524 mechanism requires competing robust models and multiple independent field observations
525 (Odbert and Wadge, 2009);

526 *iii)* assumptions behind the numerical model imply several limitations, such as those due to
527 the constant value of the dyke width and simplified Newtonian rheology. The first
528 assumption greatly oversimplifies the physics. In the case of large overpressures, stress at
529 the dyke tips will exceed the fracture toughness of the rocks and the dyke will expand
530 horizontally (Massaro et al., 2018b), reaching some equilibrium configuration. When the
531 deep chamber deflates, overpressure in the deeper dyke will decrease and, as flow rate
532 decreases, magma at the dyke tips can solidify, leading to a decrease in $2a_{0d}$ (Kavanagh and
533 Sparks, 2011; Melnik and Costa, 2014). In addition, a more realistic estimate of the magma
534 viscosity during lava dome eruptions should account for the coupling with energy loss,
535 viscous dissipation, and stick–slip effects (e.g. Costa and Macedonio, 2005; Costa et al.
536 2007c; 2013).

537

538 7. Conclusions

539 The coupling of wavelet analysis and numerical modelling allowed the deciphering of eruptive
540 behaviour of Fuego de Colima in the period 1998-2018, as revealed by satellite thermal data. Three
541 periodicities emerged from the study: i) long-term ii) intermediate-term, and, iii) short-term.



542 The long-term periodicity extracted from wavelet analysis is ca. 913-547 days (ca. 1.5-2.5 years),
543 which can be replicated by the dual magma chamber model that provided a periodicity of ca. 1000-
544 500 days. The intermediate-term periodicity obtained from wavelet analysis (ca. 146-292 days, 5-10
545 months) can be replicated by the single magma chamber model, which provides a periodicity of ca.
546 220 days. The short-term periodicity of ca. 18-38 days (ca. 2.5-5 weeks) is matched by model
547 outputs considering the dynamics of the upper conduit (ca. 16-40 days). The depicted behaviour of
548 effusive activity at Fuego de Colima is here presented for the first time, showing how the volcano
549 presents similarities with eruptive dynamics of other recent lava dome eruptions (i.e. Montserrat,
550 Costa et al., 2013).

551

552

553 Code availability

554 Melnik and Costa (2014) code is a research software and is not still available for distribution as it
555 lacks of documentation. It can be used by contacting the authors under their supervision.

556

557

558 Data availability

559 The original thermal dataset is available on www.mirovaweb.it. Excel worksheets can be obtained
560 by contacting the authors.

561

562 Appendices

563

564 **Appendix A1.** Results of the Fourier analysis. (a) The 2002-2006 period shows two main periodic
565 components, $T_0 = 24.70$ and $T_1 = 6.17$ months, corresponding to ca. 2 years and ca. 6 months,
566 respectively; (b) The 2013-2016 period shows similar results: $T_0 = 24.94$ and $T_1 = 6.23$ months,
567 corresponding to ca. 2.1 years and ca. 6 months, respectively.

568

569 **Appendix A2.** Sensitivity tests for steady state solutions of discharge rate vs chamber pressure (top)
570 and time evolution of discharge rates (bottom). These solutions are referred to the following main
571 input parameters: i) dyke thickness $2b = 40$ m as the conduit diameter at the top ($D=2b$), the
572 transition from the dyke to cylindrical conduit $L_T = 500$ m below the surface, the length of the dyke
573 $L_d = 6$ km, and the volume of the magma chamber $V_{ch} = 50 \text{ km}^3$. (a) General solution showing the
574 transient regime where the periodicity can occur; (b) Solutions influenced by the dyke width $2a$
575 (from 200 to 400 m); (c) Solutions influenced by the proportion of the water content in the melt
576 (H_2O from 4 to 5 %).



577 **Appendix A3.** Sensitivity tests for transient solutions using the single magma chamber model. As a
578 reference these solutions have the same main input parameters used for A2. (a) Dependence of
579 discharge rate on time considering the influence of the dyke width $2a$ (from 200 to 400 m); (b)
580 Influence of the magma chamber volume V_{ch} (from 20 to 50 km³); (c) Dependence of discharge rate
581 on time considering the dyke elasticity. Each curve shows a solution with a constant influx rate Q_{in}
582 (in the range of 0.01- 0.1 m³ s⁻¹).

583

584 **Appendix A4.** Sensitivity tests for transient solutions using the dual magma chamber model. The
585 shallow feeding system has dyke with a width $2a = 200$ m, $2b = 40$ m, and $L_T = 500$ m. The
586 cylindrical conduit diameter $D = 2b$. For each diagram, is indicated the outflow (Q_{out} ; black red and
587 green lines), the flux entering into the shallower magma chamber (Q_{ins} ; blue line) and periods in
588 days (T). Runs of Section 1-2-3 have $Q_{in,d} = 2.3$ (m³ s⁻¹).

589 • *Section 1*) The volumes of the shallow and deep magma chambers are fixed to 40 km³ and
590 650 km³, respectively. A set of runs is carried out for three different aspect ratios (AR) of the
591 shallow and deep chambers ($ARs = 1$; $ARd = 1$, $ARs = 2$; $ARd = 1$, $ARs = 2$; $ARd = 1.5$)
592 considering three widths of the deeper dyke ($2a_{od} = 200$ m - black line, 1000 m - red line,
593 3000 m - green line).

594 • *Section 2*) The volume of the deeper magma chamber and the aspect ratios of both shallow
595 and deep chambers are fixed to 650 km³ and $ARs = ARd = 1$. A set of runs is provided for
596 three different shallow chamber volumes ($V_{chs} = 30$ km³, 40 km³, 50 km³) considering three
597 widths of the deeper dyke ($2a_{od} = 200$ m - black line, 1000 m - red line, 3000 m - green
598 line);

599 • *Section 3*) The shallow chamber volume and the aspect ratios of both shallow and deep
600 chambers are fixed to 40 km³ and $ARs = ARd = 1$, respectively. A set of runs is carried out
601 for three deep chamber volumes ($V_{chd} = 550$ km³, 650 km³, 750 km³) considering three
602 widths of the deeper dyke ($2a_{od} = 200$ m - black line, 1000 m - red line, 3000 m - green
603 line).

604 • *Section 4*) The shallow and deep chamber volumes are fixed to 40 km³ and 650 km³,
605 respectively. Two set of runs are carried out for $Q_{in,d}$ equal to 1 and 3 (m³ s⁻¹). The aspect
606 ratios (AR) of the shallow and deep chambers are both equal to 1, considering three widths
607 of the deeper dyke ($2a_{od} = 200$ m - black line, 1000 m - red line, 3000 m - green line).

608

609

610

611

612



613 **Author's contribution**

614

615 SM and AC compiled the numerical simulations and formulated the adopted methodology. DC
616 provided and processed the satellite thermal data. LC provided the volcanological data. SM and RS
617 wrote the manuscript with the input of all the co-authors. All authors worked on the interpretation
618 of the results.

619

620

621 **Competing interests**

622 The authors declare that they have no conflict of interest.

623 **Acknowledgments**

624

625 SM thanks Centro de Geociencias of Queretaro (UNAM, Mexico) for the hospitality during the
626 period of research at Fuego de Colima volcano, the Doctoral Course in Geoscience of University of
627 Bari (Italy) for the partial financial support and Dr. F. Loparco for the help with the Python coding.
628 LC was supported by PAPIIT-UNAM n° 105116 project.

629

630 **References**

631

632 Arámbula-Mendoza, R., Lesage, P., Valdéz-Gonzales, C., Varley, N., Reyes-Dávila, G. and
633 Navarro-Ochoa, C.: Seismic activity that accompanied the effusive and explosive eruptions
634 during the 2004–2005 period at Volcán de Colima, Mexico, *J. Volcanol. Geotherm. Res.*,
635 205, 30–46, 2011.

636 Arámbula-Mendoza, R., Reyes-Dávila, G., Dulce, M. V. B., González-Amezcuca, M., Navarro-
637 Ochoa, C., Martínez-Fierros, A., and Ramírez-Vázquez, A.: Seismic monitoring of
638 effusive-explosive activity and large lava dome collapses during 2013–2015 at Volcán de
639 Colima, Mexico. *J. Volcanol. Geotherm. Res.*, 351, 75-88, 2018.

640

641 Barmin, A., Melnik, O. and Sparks, R.S.J.: Periodic behavior in lava dome eruptions, *Earth*
642 *Planet. Sci. Lett.*, 199 (1), 173-184, 2002.

643

644 Belousov, A., Voight, B., Belousova, M. and Petukhin, A.: Pyroclastic surges and flows from the 8-
645 10 May 1997 explosive eruption of Bezymianny volcano, Kamchatka, Russia, *B. Volcanol.*,
646 64 (7), 455-471, 2002.

647

648 Bernstein, M., Pavez, A., Varley, N., Whelley, P. and Calder, E.S.: Rhyolite lava dome growth
649 styles at Chaitén Volcano, Chile (2008-2009): Interpretation of thermal imagery, *Andean*
650 *Geology*, 40 (2), 2013.

651

652 Brèton-Gonzalez, M., Ramirez, J.J. and Navarro-Ochoa, C.: Summary of the historical eruptive
653 activity of Volcan de Colima, Mexico 1519-2000, *J. Volcanol. Geotherm. Res.*, 117, 21–46,
654 2002.

655



- 656 Bonasia, R., Capra, L., Costa, A., Macedonio, G., and Saucedo, R.: Tephra fallout hazard
657 assessment for a Plinian eruption scenario at Volcán de Colima (Mexico), *J. Volcanol.*
658 *Geotherm. Res.*, 203, 12-22, 2011.
659
- 660 Capra, L., Borselli, L., Varley, N., Gavilanes-Ruiz, J. C., Norini, G., Sarocchi, D., and Cortes, A.:
661 Rainfall-triggered lahars at Volcán de Colima, Mexico: surface hydro-repellency as
662 initiation process. *J. Volcanol. Geotherm. Res.*, 189 (1-2), 105-117, 2010.
663
- 664 Capra, L., Macías, J.L., Cortés, A., Dávila, N., Saucedo, R., Osorio-Ocampo, S., Arce, J.L.,
665 Galvilanes-Ruiz, J.C., Corona-Cávez, P., García-Sánchez, L., Sosa-Ceballos, G., Vasquez, R.:
666 Preliminary report on the July 10–11, 2015 eruption at Volcán de Colima: Pyroclastic
667 density currents with exceptional runouts and volume, *J. Volcanol. Geotherm. Res.*, 310,
668 39-49, 2016.
- 669 Cazelles, B., Chavez, M., Berteaux, D., Ménard, F., Vik, J. O., Jenouvrier, S., and Stenseth, N.C.:
670 Wavelet analysis of ecological time series. *Oecologia*, 156(2), 287-304, 2008.
671
- 672 Christopher, T.E., Blundy, J., Cashman, K., Cole, P., Edmonds, M., Smith, P. J., and Stinton, A.:
673 Crustal-scale degassing due to magma system destabilization and magma-gas decoupling
674 at Soufrière Hills Volcano, Montserrat. *Geochem. Geophys. Geosyst.*, 16(9), 2797-2811,
675 2015.
- 676 Coppola, D., Piscopo, D., Staudacher, T. and Cigolini, C.: Lava discharge rate and effusive
677 pattern at Piton de la Fournaise from MODIS data. *J. Volcanol. Geotherm. Res.*, 184 (1–2),
678 174–192, 2009.
- 679 Coppola, D., Laiolo, M., Piscopo, D. and Cigolini, C.: Rheological control on the radiant
680 density of active lava flows and domes. *J. Volcanol. Geotherm. Res.*, 249, 39-48, 2013.
681
- 682 Coppola, D., Laiolo, M., Cigolini, C., Delle Donne, D., and Ripepe, M.: Enhanced volcanic hot-
683 spot detection using MODIS IR data: results from the MIROVA system. *Geol. Soc.*
684 *London, Special Publications*, 426(1), 181-205, 2016.
685
686
- 687 Costa A. and Macedonio, G: Viscous heating in fluids with temperature-dependent viscosity:
688 Triggering of secondary flows, *J. Fluid Mech.*, 540, 21– 38, 2005.
689
- 690 Costa, A., Melnik, O., Sparks, R.S.J.: Controls of conduit geometry and wallrock elasticity on lava
691 dome eruptions, *Earth Planet. Sci. Lett.*, 260, 137–151, 2007a.
692
- 693 Costa, A., Melnik, O., Sparks R.S.J. and Voight, B.: Control of magma flow in dykes on
694 cyclic lava dome extrusion, *Geophys. Res. Lett.*, 34 (2), 2007b.
695
- 696 Costa, A., Melnik, O. and Vedeneva, E.: Thermal effects during magma ascent in conduits, *J.*
697 *Geophys. Res.*, Vol. 112, B12205, 2007c.
698
- 699 Costa A., Caricchi L., Bagdassarov N.: A model for the rheology of particle-bearing
700 suspensions and partially molten rocks, *Geochem. Geophys. Geosyst.*, 10, Q03010,
701 doi:10.1029/2008GC002138, 2009.
702



- 703 Costa, A., Wadge, G., Melnik, O.: Cyclic extrusion of a lava dome based on a stick-slip
704 mechanism. *Earth Planet. Sci. Lett.*, 337, 39-46, 2012.
705
- 706 Costa, A., Wadge, G., Stewart, R., Odbert, H.: Coupled subdaily and multiweek cycles during the
707 lava dome eruption of Soufrière Hills Volcano, Montserrat. *J. Geophys. Res., Solid Earth*,
708 118(5), 1895-1903, 2013.
709
- 710 Clavijero, F.X.: *Historia Antigua de Mexico*, Sepan Cuantos, 29, Porrúa, 1780.
711
- 712 Cortés, A., Garduño-Monroy, V.H., Navarro-Ochoa, C., Komorowski, J.C., Saucedo, R., Macías,
713 J.L. and Gavilanes, J.C.: Carta geológica del Complejo Volcánico de Colima, con
714 Geología del Complejo Volcánico de Colima, Univer. Nat. Autón. México, Inst. Geol.,
715 Cartas Geológicas y Mineras, 10, 2005.
- 716 Daubechies: *Ten Lectures on Wavelets*. Society for Industrial and Applied Mathematics, 357, 1992.
- 717 De Bélizal, É., Lavigne, J.C., Gaillard, D., Grancher, I., Pratomo, I., and Komorowski, J.C.: The
718 2007 eruption of Kelut volcano (East Java, Indonesia): phenomenology, crisis
719 management and social response, *Geomorphology*, 136(1), 165-175, 2012.
720
- 721 De la Cruz-Reyna, S.: Random patterns of activity of Colima Volcano, Mexico, *J. Volcanol.*
722 *Geotherm. Res.*, 55, 51–68, 1993.
723
- 724 Denlinger, R.P. and Hoblitt, R.P.: Cyclic eruptive behavior of silicic volcanoes, *Geology*, 27 (5),
725 459-462 1999.
726
- 727 Dragoni, M. and Tallarico, A.: Assumption in the evaluation of lava effusion rates from heat
728 radiation. *Geoph. Res. Lett.*, 36, L08302, 2009.
- 729 Farge, M.: Wavelet transforms and their applications to turbulence. *Annu. Rev. Fluid Mech.*, 24,
730 395–457, 1992.
- 731 Farquharson, J., Heap, M.J., Varley, N. R., Baud, P. and Reuschlé, T.: Permeability and porosity
732 relationships of edifice-forming andesites: a combined field and laboratory study. *J. Volcanol.*
733 *Geotherm. Res.*, 297, 52-68, 2015.
734
- 735 Fougere, P.: On the accuracy of spectrum analysis of red noise processes using maximum entropy
736 and periodogram models: simulation studies and application to geophysical data. *J.*
737 *Geophys. Res.* 90, 4355–4366, 1985.
- 738
- 739 Garel, F., Kaminski, E., Tait, S., Limare, A.: An experimental study of the surface thermal
740 signature of hot subaerial isoviscous gravity currents: implications for thermal monitoring of
741 lava flows and domes. *J. Volcanol. Geotherm. Res.*, 117, B02205, 2012.
- 742 Gavilanes-Ruiz, J.C., Cuevas-Muñiz, A., Varley, N., Gwynne, G., Stevenson, J., Saucedo-Girón,
743 R., and Cortés-Cortés, A.: Exploring the factors that influence the perception of risk: The
744 case of Volcán de Colima, Mexico, *J. Volcanol. Geotherm. Res.*, 186(3), 238-252, 2009.
745
- 746 Global Volcanism Program: Report on Colima (Mexico). In: Wunderman, R (ed.), *B. Global*
747 *Volcanism Net.*, 23-10, Smithsonian Institution, 1998.
748



- 749 Global Volcanism Program: Report on Colima (Mexico). In: Wunderman, R (ed.), Bulletin of the
750 Global Volcanism Network, 25-6, Smithsonian Institution, 2000.
751
- 752 Global Volcanism Program: Report on Colima (Mexico). In: Wunderman, R (ed.), B. Global
753 Volcanism Net., 27-11, Smithsonian Institution, 2002.
754
- 755 Global Volcanism Program: Report on Colima (Mexico). In: Venzke, E (ed.), B. Global
756 Volcanism Net., 28-11, Smithsonian Institution, 2003.
757
- 758 Global Volcanism Program: Report on Colima (Mexico). In: Wunderman, R (ed.), B. Global
759 Volcanism Net., 38-12, Smithsonian Institution, 2013.
760
- 761 Global Volcanism Program: Report on Colima (Mexico). In: Sennert, S K (ed.), Weekly Volcanic
762 Activity Report, 26 July-1 August 2017, Smithsonian Institution and US Geological Survey,
763 2017.
764
- 765 Harris, A.J., Rose, W.I. and Flynn, L.P.: Temporal trends in lava dome extrusion at Santiaguito
766 1922-2000, *B. Volcanol.*, 65(2), 77-89, 2003.
767
- 768 Harris, A.J.L., Rowland, S.K.: Effusion rate controls on lava flow length and the role of heat
769 loss: a review. In: Thordarson, T., Self, S., Larsen, G., Rowland, S.K., Hoskuldsson, A.
770 (Eds.), *Studies in Volcanology: The Legacy of George Walker: Special Publication*
771 *IAVCEI*, 2, pp. 33–51, 2009.
- 772 Harris, A.J.L., Favalli, M., Steffke, A., Fornaciai, A., Boschi, E.: A relation between lava
773 discharge rate, thermal insulation, and flow area set using lidar data. *Geoph. Res.*
774 *Lett.*, 37, L20308. <http://dx.doi.org/10.1029/2010GL044683>, 2010.
- 775 Heap, M.J., Lavallée, Y., Petrakova, L., Baud, P., Reuschle, T., Varley, N., and Dingwell D.B.:
776 Microstructural controls on the physical and mechanical properties of edifice-forming
777 andesites at Volcán de Colima, Mexico, *Solid Earth*, 119 (4), 2925-2963, 2014.
778
- 779 Hutchison, W., Varley, N., Pyle, D.M., Mather, T.A., and Stevenson, J.A.: Airborne thermal
780 remote sensing of the Volcán de Colima (Mexico) lava dome from 2007 to 2010, *Geol. Soc.*
781 *London, Spec. Public.*, 380 (1), 203-228, 2013.
782
- 783 James, M. R. and Varley, N.: Identification of structural controls in an active lava dome with high
784 resolution DEMs: Volcán de Colima, Mexico. *Geoph. Res.Lett.*, 39(22), 2012.
785
- 786 Kavanagh, J. L. and Sparks, R.S.J.: Insights of dyke emplacement mechanics from detailed 3D dyke
787 thickness datasets. *J.Geol. Soc.*, 168(4), 965-978, 2011.
788
- 789 Kozono, T. and Koyaguchi, T.: Effects of gas escape and crystallization on the complexity of
790 conduit flow dynamics during lava dome eruptions. *Geoph. Res.Lett.*, *Solid Earth*, 117(B8),
791 2012.
792
- 793 Lamb, O.D., Varley, N., Mather, T.A., Pyle, D.M., Smith, P.J. and Liu, E.J.: Multiple timescales of
794 cyclical behaviour observed at two dome-forming eruptions, *J. Volcanol. Geotherm. Res.*,
795 284, 106-121, 2014.
796
- 797 Lau K.M. and Weng H.: Climatic signal detection using wavelet transform: how to make a time
798 series sing. *Bull Am Meteorol Soc.*, 76. 2391–2402, 1995.



- 799 Lavallée, Y., Varley, N., Alatorre-Ibargüengoitia, M.A., Hess, K.U., Kueppers, U., Mueller, S.,
800 Richard, D., Scheu, B., Spieler, O. and D.B. Dingwell, D.B.: Magmatic architecture of
801 dome-building eruptions at Volcan de Colima (Mexico), *Bull. Volcanol.*, 74 (1), 249-260,
802 2012.
803
- 804 Lensky, N.G., Navon, O. and Lyakhovsky, V.: Bubble growth during decompression of magma:
805 experimental and theoretical investigation, *J. Volcanol. Geotherm. Res.*, 129 (1), 7-22, 2004.
806
- 807 Loughlin, S.C., Luckett, R., Ryan, G., Christopher, T., Hards, V., De Angelis, S. and Strutt, M.: An
808 overview of lava dome evolution, dome collapse and cyclicity at Soufrière Hills Volcano,
809 Montserrat, 2005–2007, *Geophys. Res. Lett.*, 37 (19), 2010.
810
- 811 Luhr, J.F. and Carmichael, I.S.: The Colima Volcanic Complex, Mexico, *Con.to Mineral.Petrol.*, 71
812 (4), 343-372, 1980.
813
- 814 Luhr, J.F.: Petrology and geochemistry of the 1991 and 1998-1999 lava flows from Volcan
815 Colima, Mexico, *J. Volcanol. Geotherm. Res.*, 117, 169–194, 2002.
816
- 817 Macias, J., Arce, J., Sosa, G., Gardner, J.E., Saucedo, R.: Storage conditions and magma
818 processes triggering the 1818CE Plinian eruption of Volcán de Colima, *J. Volcanol.*
819 *Geotherm. Res.*, doi:10.1016/j.jvolgeores.2017.02.025, 2017.
- 820 Mallat, S.: A wavelet tour of signal processing. Academic Press, San Diego, 1998.
- 821 Massaro, S., Sulpizio, R., Costa, A., Capra, L., Lucchi, F.: Understanding eruptive style variations
822 at calc-alkaline volcanoes: the 1913 eruption of Fuego de Colima volcano (Mexico), *B.*
823 *Volcanol.*, 80-62, <https://doi.org/10.1007/s00445-018-1235-z>, 2018a.
- 824 Massaro, S., Costa, A., Sulpizio, R.: Time evolution of a magma feeding system during a Plinian
825 eruption: the example of the Pomici di Avellino eruption of Somma-Vesuvius (Italy), *Earth*
826 *Planet. Sci. Lett.* 482, 545-555, 2018b.
827
- 828 Medina-Martinez, F.: Analysis of the eruptive history of the Volcán de Colima, Mexico (1560–
829 1980), *Geofísica Internacional*, 22, 157–178, 1983.
830
- 831 Martin del Pozzo, A.L., Sheridan, M., Barrera, D., Lugo Hubp, J. and Vázquez Selem, L.:
832 Potential hazards from Colima volcano, Mexico, *Geofísica Internacional*, 34 (4), 363-376.
833 1995.
834
- 835 Melnik, O. and Sparks, R.S.J.: Nonlinear dynamics of lava dome extrusion, *Nature*, 402
836 (6757), 37-41, 1999.
837
- 838 Melnik, O. and Sparks, R.S.J.: Dynamics of magma ascent and lava extrusion at Soufrière
839 Hills Volcano, Montserrat, *Geol. Soc. London Mem.*, 21 (1), 153-171, 2002.
840
- 841 Melnik, O. and Sparks, R.S.J.: Controls on conduit magma flow dynamics during lava-dome
842 building eruptions, *J. Geophys. Res.*, 110, B02209, doi:10.1029/2004JB003183, 2005.
- 843 Melnik, O., Sparks, R.S.J., Costa, A. and Barmin, A.: (2008), Volcanic Eruptions: Cyclicity during
844 Lava Dome Growth, in Meyers: *Encyclopedia of Complexity and Systems Science*, 2008.



- 845 Melnik, O. and A. Costa, A.: Dual-chamber-conduit models of non-linear dynamics behaviour at
846 Soufrière Hills Volcano, Montserrat, *Geol. Soc. Lond., Mem.*, 39, 61-69, 2014.
847
- 848 Mériaux, C. and Jaupart, C.: Simple fluid dynamic models of volcanic rift zones, *Earth Planet. Sci.*
849 *Lett.*, 136(3-4), 223-240, 1995.
850
- 851 Mora, J. C., Macias, J. L., Saucedo, R., Orlando, A., Manetti, P., and Vaselli, O.: Petrology of the
852 1998–2000 products of Volcán de Colima, México. *J. Volcanol. Geotherm. Res.*, 117(1),
853 195-212, 2002.
854
- 855 Mueller, S.B., Varley, N., Kueppers, U., Lesage, P. and Reyes-Dávila, G.: Quantification of
856 magma ascent rate through rockfall monitoring at the growing/collapsing lava dome of
857 Volcan de Colima, Mexico, *Solid Earth*, 4, 201-213, 2013.
858
- 859 Nakanishi, M. and Koyaguchi, T.: A stability analysis of a conduit flow model for lava dome
860 eruptions. *J. Volcanol. Geotherm. Res.*, 178(1), 46-57, 2008.
861
- 862 Nakada, S., Shimizu, H. and Ohta, K.: Overview of the 1990–1995 eruption at Unzen Volcano, *J.*
863 *Volcanol. Geotherm. Res.*, 89 (1), 1-22, 1999.
864
- 865 Navarro-Ochoa, C., Gavilanes-Ruiz, A. Cortès-Cortès, A.: Movement and emplacement of lava
866 flows at Volcán de Colima, México: November 1998–February 1999, *J. Volcanol.*
867 *Geotherm. Res.*, 117 (1), 155-167, 2002.
- 868 Nicholson, R.S., Gardner, J.E., and Neal, C.A.: Variations in eruption style during the 1931 A.D.
869 eruption of Aniakchak volcano, Alaska, *J. Volcanol. Geotherm. Res.*, 207, 69–82, 2011.
- 870 Norini, G., Capra, L., Groppelli, G., Agliardi, F., Pola, A., and Cortès, A.: Structural architecture of
871 the Colima Volcanic Complex, *J. Geophys. Res.*, 115, B12209, 2010.
872
- 873 Odbert, H.M. and Wadge, G.: Time series analysis of lava flux. *J. Volcanol. Geotherm. Res.*,
874 188(4), 305-314, 2009.
875
- 876 Ozerov, A., Ispolatov, I. and Lees, J.: Modeling strombolian eruptions of Karymsky volcano,
877 Kamchatka, Russia, *J. Volcanol. Geotherm. Res.*, 122 (3), 265-280, 2003.
878
- 879 Ramsey, M.S. and Harris, A.J.L.: Volcanology 2020: how will thermal remote sensing of
880 volcanic surface activity evolve over the next decade? *J. Volcanol. Geotherm. Res.*,
881 <http://dx.doi.org/10.1016/j.jvolgeores.2012.05.011>, 2012.
- 882 Reyes-Dávila, G.A., Arámbula-Mendoza, R., Espinasa-Pereña, P., Pankhurst, M.J., Navarro-
883 Ochoa, C., Savov, I. and Domínguez-Reyes, T.: Volcán de Colima dome collapse of
884 July, 2015 and associated pyroclastic density currents, *J. Volcanol. Geotherm. Res.*, 320,
885 100-106, 2016.
886
- 887 Reubi, O. and Blundy, J.: Assimilation of Plutonic roots, formation of high-K exotic melt
888 inclusions and genesis of andesitic magmas at Volcán De Colima, Mexico, *J. Petrol.* 49, 12,
889 2221–2243, 2008.
890
- 891 Reubi, O., Blundy, J. and Varley, N.: Volatiles contents, degassing and crystallisation of
892 intermediate magmas at Volcán de Colima, Mexico, inferred from melt inclusions.



- 893 Contr. Mineral. Petrol., 165(6), 1087-1106, 2013.
- 894 Reubi, O., Sims, K.W., Varley, N., Reagan, M. and Eikenberg, J.: Timescales of degassing and
895 conduit dynamics inferred from ^{210}Pb – ^{226}Ra disequilibria in Volcán de Colima 1998–
896 2010 andesitic magmas. *Geol. Soc., London, Sp. Publ.*, 422, SP422-5, 2015.
- 897
- 898 Salzer, J.T., Nikkhoo, M., Walter, T.R., Sudhaus, H., Reyes-Dávila, G., Bretón, M. and Arámbula,
899 R.: Satellite radar data reveal short-term pre-explosive displacements and a complex conduit
900 system at Volcán de Colima, Mexico, *Frontiers in Earth Sci.*, 2, 12, 2014.
- 901
- 902 Saucedo, R., Macías, J.L., Sheridan, M.F., Bursik, M.I., Komorowski, J.C.: Modeling of
903 pyroclastic flows of Colima Volcano, Mexico: implications for hazard assessment, *J.*
904 *Volcanol. Geotherm. Res.*, 139 (1–2), 103–115, 2005.
- 905
- 906 Saucedo, R., J.L. Macías, J.C. Gavilanes, J.L. Arce, J.C. Komorowski, J.E. Gardner, and G.
907 Valdez-Moreno, G.: Eyewitness, stratigraphy, chemistry, and eruptive dynamics of the
908 1913 Plinian eruption of Volcán de Colima, México, *J. Volcanol. Geotherm. Res.*, 191(3),
909 149-166, 2010.
- 910
- 911 Savov, I.P., Luhr, J.F. and Navarro-Ochoa, C.; Petrology and geochemistry of lava and ash
912 erupted from Volcan Colima, Mexico, during 1998-2005, *J. Volcanol. Geotherm. Res.*, 174,
913 241–256, 2008.
- 914
- 915 Siswowardjyo, S., Suryo, I. and Yokoyama, I.: Magma eruption rates of Merapi volcano,
916 Central Java, Indonesia during one century (1890–1992), *B. Volcanol.*, 57 (2), 111-116,
917 1995.
- 918
- 919 Sparks, R.S.J.: Causes and consequences of pressurisation in lava dome eruptions, *Earth Planet. Sci.*
920 *Lett.*, 150 (3-4), 177-189, 1997.
- 921
- 922 Sparks, R.S.J. and Young, S.R.: The eruption of Soufrière Hills volcano, Montserrat (1995–1999):
923 Overview of scientific results, in *The Eruption of the Soufrière Hills Volcano, Montserrat*
924 *from 1995 to 1999*, *Geol. Soc. London Mem.*, 21, 45– 69, 2002.
- 925
- 926 Spica, Z., Perton, M. and Legrand, D.: Anatomy of the Colima volcano magmatic system,
927 Mexico, *Earth Planet. Sci. Lett.*, 459, 1-13, 2017.
- 928
- 929 Sulpizio, R., Capra, L., Sarocchi, D., Saucedo, R., Gavilanes-Ruiz, J. C. and Varley, N.: Predicting
930 the block-and-ash flow inundation areas at Volcán de Colima (Colima, Mexico) based on
931 the present day (February 2010) status. *J. Volcanol. Geotherm. Res.*, 193(1-2), 49-66, 2010.
- 932
- 933 Swanson, D.A. and Holcomb, R.T.: Regularities in growth of the Mount St. Helens dacite
934 dome, 1980–1986, in *Lava Flows and Domes: Emplacement Mechanisms and Hazard*
935 *Implications*, 3-24, 1990.
- 936
- 937 Thiele, S.T., Varley, N. and James, M.R.: Thermal photogrammetric imaging: A new technique for
938 monitoring dome eruptions, *J. Volcanol. Geotherm. Res.*, 337, 140-145, 2017.
- 939
- 940 Trauth, M.: *MATLAB Recipes for Earth Sciences*, 1st ed. Springer-Verlag, Berlin Heidelberg,
941 2006.



- 942 Torrence, C. and Compo, G.P.: A practical guide to wavelet analysis. *Bulletin of the American*
943 *Meteorological society*, 79(1), 61-78, 1998.
- 944
- 945 Varley, N., Arámbula-Mendoza, R., Reyes-Dávila, G., Stevenson, J., Harwood, R.: Long-
946 period seismicity during magma movement at Volcán de Colima, B. *Volcanol.*, 72, 1093–
947 1107. <http://dx.doi.org/10.1007/s00445-010-0390-7>, 2010a.
- 948
- 949 Varley, N., Arámbula-Mendoza, R., Reyes-Reyes-Dávila, G., Sanderson, R., Stevenson, J.:
950 Generation of Vulcanian activity and long-period seismicity at Volcan de Colima, Mexico.
951 *J. Volcanol. Geotherm. Res.*, 198, 45–56, 2010b.
- 952 Varley, N: La evolución de la actividad reciente del Volcán de Colima, webseminar, Unión
953 Geofísica Mexicana A.C., 2015.
- 954
- 955 Vila, J., Macià, R., Kumar, D., Ortiz, R., Moreno, H., Correig, A.: Analysis of the unrest of active
956 volcanoes using variations of the base level noise seismic spectrum. *J. Volcanol. Geotherm.*
957 *Res.* 153, 11–20, 2006.
- 958 Voight, B., Hoblitt, R.P., Clarke, A.B., Lockhart, A. Miller, L. Lynch and McMahon, J.:
959 Remarkable cyclic ground deformation monitored in real-time on Montserrat, and its use
960 in eruption forecasting, *Geophys. Res. Lett.*, 25 (18), 3405-3408, 1998.
- 961
- 962 Voight, B., Sparks, R.S.J., Miller, A.D., Stewart, R.C., Hoblitt, R.P., Clarke, A. and Cole, P.:
963 Magma flow instability and cyclic activity at Soufriere Hills volcano, Montserrat,
964 british west indies, *Science*, 283 (5405), 1138-1142, 1999.
- 965
- 966 Voight, B., Constantine, E.K., Siswowardjoyo, S. and Torley, R.: Historical eruptions of Merapi
967 volcano, central Java, Indonesia, 1768–1998, *J. Volcanol. Geotherm. Res.*, 100 (1), 69-138,
968 2000.
- 969
- 970 Wadge, G., Dorta, D.O. and Cole, P.D.: The magma budget of Volcán Arenal, Costa Rica
971 from 1980 to 2004, *J. Volcanol. Geotherm. Res.*, 157 (1), 60-74, 2006.
- 972
- 973 Wadge, G., Herd, R., Ryan, G., Calder, E.S. and Komorowski, J.C.: Lava production at Soufrière
974 Hills Volcano, Montserrat: 1995–2009, *Geophys. Res. Lett.*, 37 (19), 2010.
- 975
- 976 Watts, R.B., Herd, R.A., Sparks, R.S.J. and Young, S.R.: Growth patterns and emplacement of the
977 andesitic lava dome at Soufriere Hills Volcano, Montserrat, *Geol. Soc. Lond. Mem.* 21(1),
978 115-152, 2002.
- 979
- 980 Weng, H. and Lau, K.M.: Wavelets, period doubling, and time-frequency localization with
981 application to organization of convection over the tropical western Pacific. *J. Atmos. Sci.*,
982 51, 2523–2541, 1994.
- 983 Wolpert, R., Ogburn, L. and Calder, E.S.: The longevity of lava dome eruptions. *Journal of*
984 *Geophysical Research: Solid Earth*, 121(2), 676-686, 2016.
- 985
- 986 Wylie, J.J., Voight, B. and Whitehead, J.A.: Instability of magma flow from volatile dependent
987 viscosity, *Science*, 285, 1883–1885 1999.



988 Zobin, V.M., Orozco-Rojas, J., Reyes-Dávila, G.A. and Navarro-Ochoa, C.: Seismicity of an
989 andesitic volcano during block-lava effusion: Volcán de Colima, México, November 1998–
990 January 1999, *Bull. Volcanol.* 67 (7), 679-688, 2005.
991
992 Zobin, V.M., Varley, N., González, M., Orozco, J., Reyes, G.A., Navarro-Ochoa, C. and M.
993 Bretón: Monitoring the 2004 andesitic block-lava extrusion at Volcán de Colima,
994 México from seismic activity and SO₂ emission, *J. Volcanol. Geotherm. Res.*, 177 (2), 367-
995 377, 2008.
996
997 Zobin, V.M., R. Arámbula, R., Bretón, M., Reyes, G., I. Plascencia, I., Navarro-Ochoa, C. and
998 Martínez, A.: Dynamics of the January 2013–June 2014 explosive-effusive episode in the
999 eruption of Volcán de Colima, México: insights from seismic and video monitoring, *Bull.*
.000 *Volcanol.* 77(4), 31, 2015.
.001
.002
.003
.004
.005
.006
.007
.008
.009
.010
.011
.012
.013
.014
.015
.016
.017
.018
.019
.020
.021
.022
.023
.024
.025
.026
.027
.028
.029
.030
.031
.032
.033
.034
.035
.036
.037
.038

.039 **Tables**

.040

Table 1: Input parameters used in numerical simulations.

Notation	Description	Value
c_o	Concentration of dissolved gas (wt.%)	0.05-0.06
C_f	Solubility coefficient ($\text{Pa}^{-1/2}$)	4.1×10^{-6}
C_m	Specific heat ($\text{J kg}^{-1} \text{K}^{-1}$)	1.2×10^3
I_0	Max nucleation rate ($\text{m}^{-3} \text{s}^{-1}$)	3×10^{10}
L_*	Latent heat of crystallization (J kg^{-1})	3.5×10^5
μ_g	Gas viscosity (Pa s)	1.5×10^{-5}
ρ_m	Density of the melt phase (kg m^{-3})	2300-2500
ρ_c	Density of the crystal (kg m^{-3})	2700-2800
T_{ch}	Temperature in the magma chamber (K)	1150
P_{ch}	Pressure in the magma chamber (MPa)	130 - 210
β_{ch}^*	Crystal content in magma chamber	0.35-0.45
ρ_r	Host rock density (kg m^{-3})	2600
G	Host rock rigidity (GPa)	6
ν	Poisson's ratio	0.25
ε		8.6

Conduit geometry parameters using a single magma chamber model

D	Diameter of the cylindrical conduit	30-40
L_T	Dyke-cylinder transition depth (m)	1300-500
$2a$	Width of the dyke (m)	200 – 600
$2b$	Thickness of the dyke (m)	4-40
L	Depth of the magma chamber (top) (m)	5500-6500
V_{ch}	Chamber volume (km^3)	20-50
AR	Aspect ratio of the magma chamber	1-2
$Q_{in,s}$	Influx into the shallow magma chamber ($\text{m}^3 \text{s}^{-1}$)	0.01-3.5

*Parameters used for simulations carried out with dual magma chamber model**Deep magma chamber*

$2a_{od}$	Width of the deeper dyke (m)	200 – 3000
L_0	Depth of the deep magma chamber (top) (m)	15000
AR_d	Aspect ratio of the deep magma chamber	1-2
V_{chd}	Deep chamber volume (km^3)	550-750
ΔP	Deep magma chamber overpressure (MPa)	20
$Q_{in,d}$	Influx into the shallow magma chamber ($\text{m}^3 \text{s}^{-1}$)	1-3



.041 **Figures Captions**

.042 **Fig. 1.** (a) Digital elevation model of the Colima Volcanic Complex (NC = Nevado de Colima
.043 volcano; FC = Fuego de Colima volcano) and Colima Rift with the main tectonic and volcano-
.044 tectonic structures (modified from Norini et al. 2010). In the inset, the location of the Colima
.045 Volcanic Complex (CVC) within the Trans-Mexican Volcanic Belt (TMVB) is shown in the frame
.046 of the subduction-type geodynamic setting of Central America. (b) Schematic view of the conduit
.047 feeding system framework used for numerical simulations (modified after Melnik and Costa, 2014).

.048 **Fig. 2.** Dataset about the averaged discharge rates of Fuego de Colima during 1998-2018, derived
.049 by the MIROVA thermal data (black points) and published data (blue crosses) (Navarro-Ochoa et
.050 al., 2002; Zobin et al., 2005; Reubi et al 2013; Mueller et al., 2013; Varley, 2015; Reyes-Dávila et
.051 al., 2016; Theiele et al., 2017; GVP, 2002-2017). Values $> 0.1 \text{ (m}^3 \text{ s}^{-1}\text{)}$ are considered to be as
.052 “high” (dark blue area) and values $< 0.1 \text{ (m}^3 \text{ s}^{-1}\text{)}$ as “low” discharge rate (light blue area). The 0.01
.053 $\text{(m}^3 \text{ s}^{-1}\text{)}$ is the threshold under which the MIROVA system does not provide reliable data (blue line);
.054 (a) Weekly average discharge rates. The boxes contain symbols of volcanological observations
.055 reported in literature; (b) Monthly average discharge rates; (c) Yearly average discharge rates.

.056 **Fig. 3.** (a) Local wavelet power spectrum normalized by $1/\sigma^2$ (σ^2 in $\text{(m}^3 \text{ s}^{-1}\text{)}^2$). The left axis is the
.057 period (in years). The bottom axis is time (in years). The shaded contours are at normalized
.058 variances of 0.5, 1, 2, and 4 $\text{(m}^3 \text{ s}^{-1}\text{)}^2$. The black thick contour encloses regions of greater than 95%
.059 confidence for a red-noise process with a lag-1 coefficient of 0.72. It shows three orders of
.060 periodicities of: long-term (ca. 1.5-2.5 years), intermediate-term (ca. 5-10 months) during 2002-
.061 2006 and 2013-2016, and short-term (ca. 2.5-5 weeks) during 2001-2006 and 2011-2016. Blue line
.062 indicates the “cone of influence” where edge effects become important outside it; (b) Global
.063 wavelet power spectrum. The green dotted line represents the best-fitting red noise spectrum at the
.064 95% confidence level.

.065 **Fig. 4.** Results of numerical simulations. The physical framework of the conduit feeding system has
.066 deep and shallow chambers connected to surface via vertical elastic dykes evolving into non-elastic
.067 cylinder. The length of the shallow dyke L_{ds} is in the range of 5500-6500 m. The passage to cylinder
.068 conduit L_c occurs at ca. 1300-500 m below the cone. (a) Discharge rates vs. time considering the
.069 elasticity of the shallower dyke, with a width $2a = 400$ m and thickness $2b = 2$ m. The cylinder
.070 diameter $D = 30$ m. Two cases are shown: *i*) constant pressure (blue line) and *ii*) constant influx rate
.071 at the source region of the dyke, providing different periodicities of 16 and 40 days, in good
.072 agreement with the short-term (weekly) periodicities observed in Fig. 3a; (b) Discharge rate vs. time



.073 using the single magma chamber model. The dyke width $2a = 600$ and thickness $2b = 4$ m. The
.074 chamber has a volume $V_{ch} = 30 \text{ km}^3$, receiving a constant influx $Q_{in,s} = 2.3 \text{ (m}^3 \text{ s}^{-1}\text{)}$; Periodicity is of
.075 ca. 220 days, in good agreement with the intermediate-term (monthly) periodicities observed in Fig.
.076 3a; (c) Discharge rate vs. time using the dual magma chamber model. The aspect ratio of the
.077 shallow and deep chambers ($AR_s - AR_d$) are both equal to 1.3 and 1.4, respectively. The upper
.078 feeding system has a chamber ($V_{chs} = 30 \text{ km}^3$) connected to a dyke (width $2a = 260$ m; $2b = 4$ m)
.079 evolving into a cylinder ($D = 30$ m) at $L_T = 1000$ m. The shallow chamber is connected to the deep
.080 one ($V_{chd} = 500 \text{ km}^3$) through a feeder dyke ($2a_{od} = 500$ m). A constant $Q_{in,d} = 2.3 \text{ (m}^3 \text{ s}^{-1}\text{)}$ is
.081 injected from below. Periodicity is in the range of ca. 825 days, in good agreement with the long-
.082 term (yearly) periodicities observed in Fig. 3a.

.083

.084

.085

.086

.087

.088

.089

.090

.091

.092

.093

.094

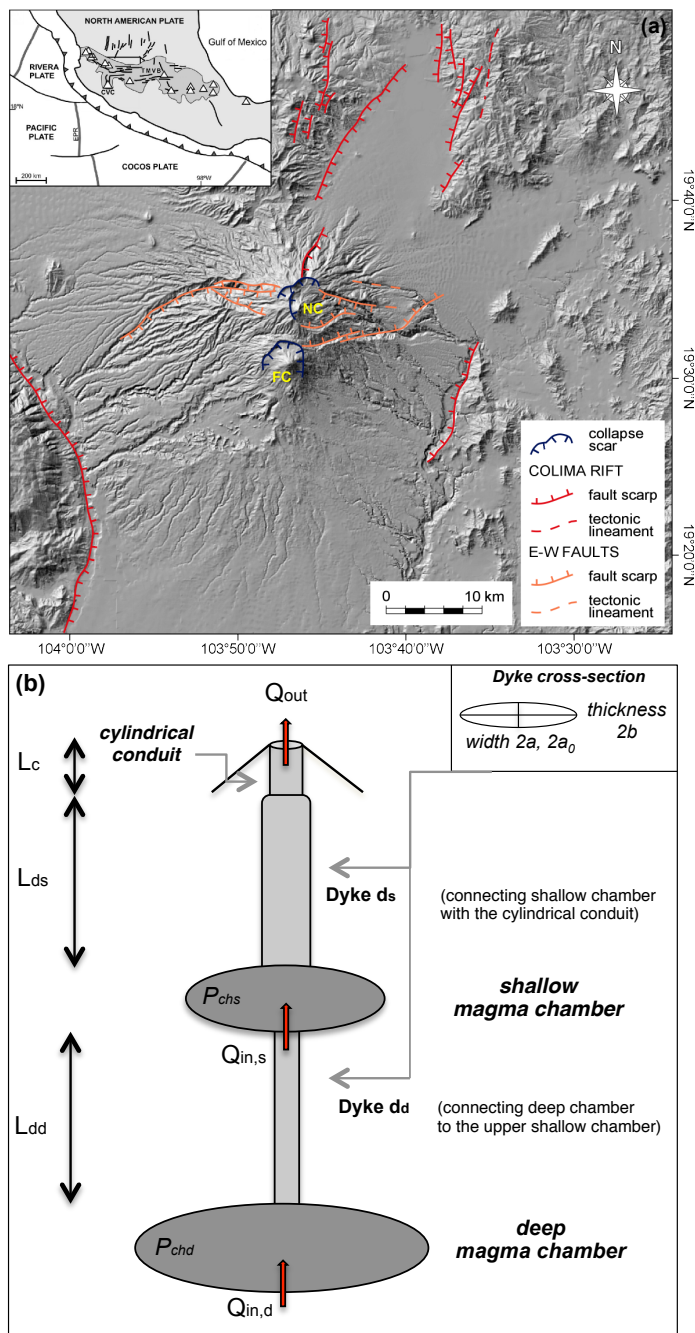
.095

.096

.097

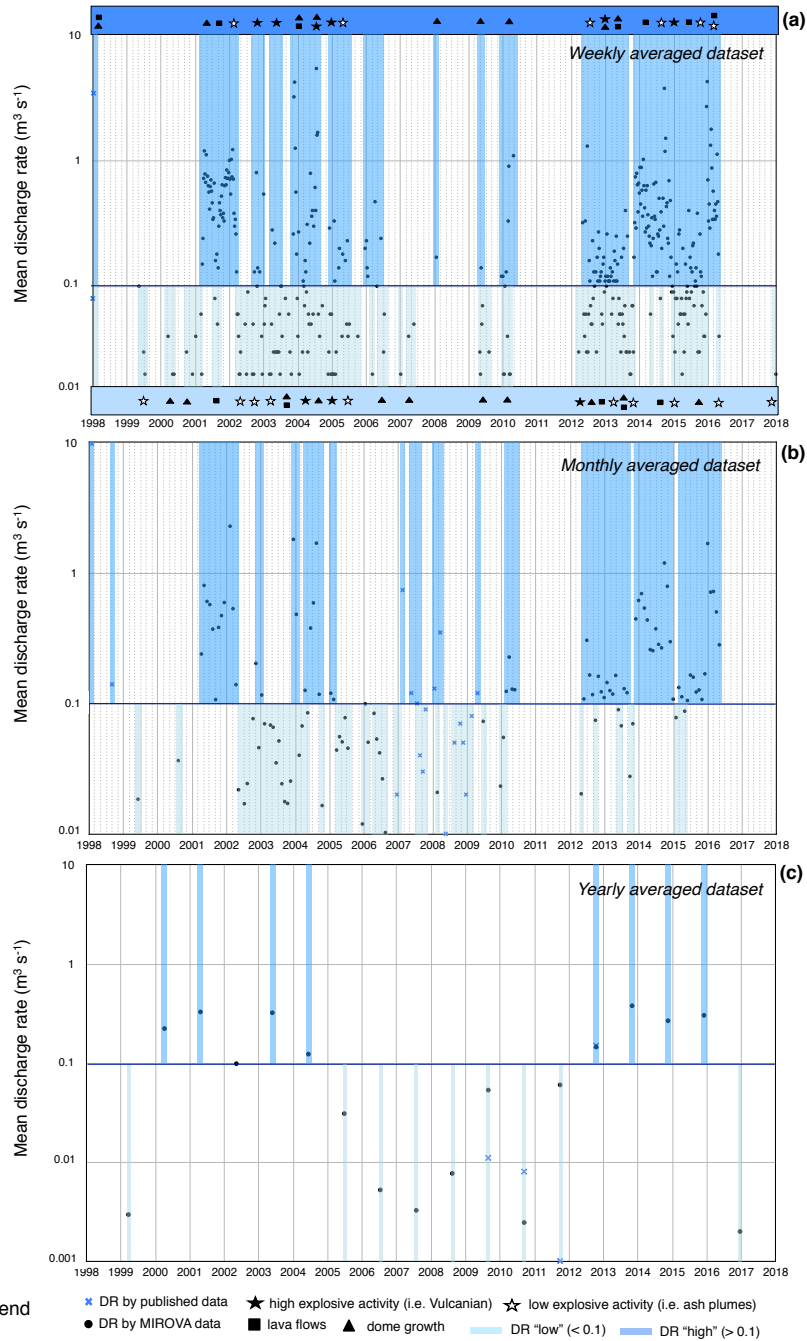


.098 Fig.1





100 Fig. 2

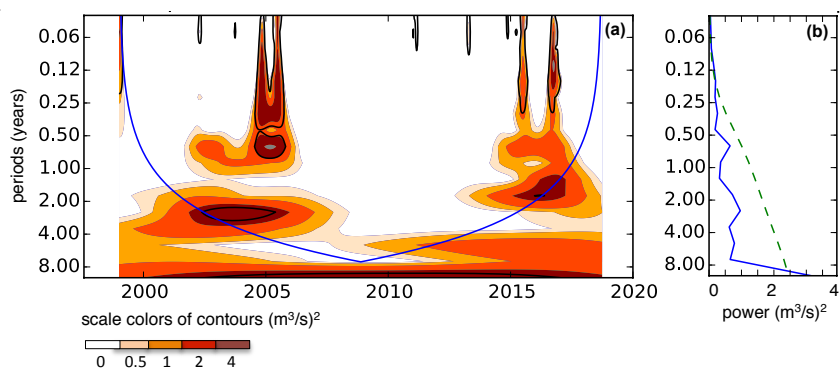


101

102



.103 Fig. 3



.104

.105

.106

.107

.108

.109

.110

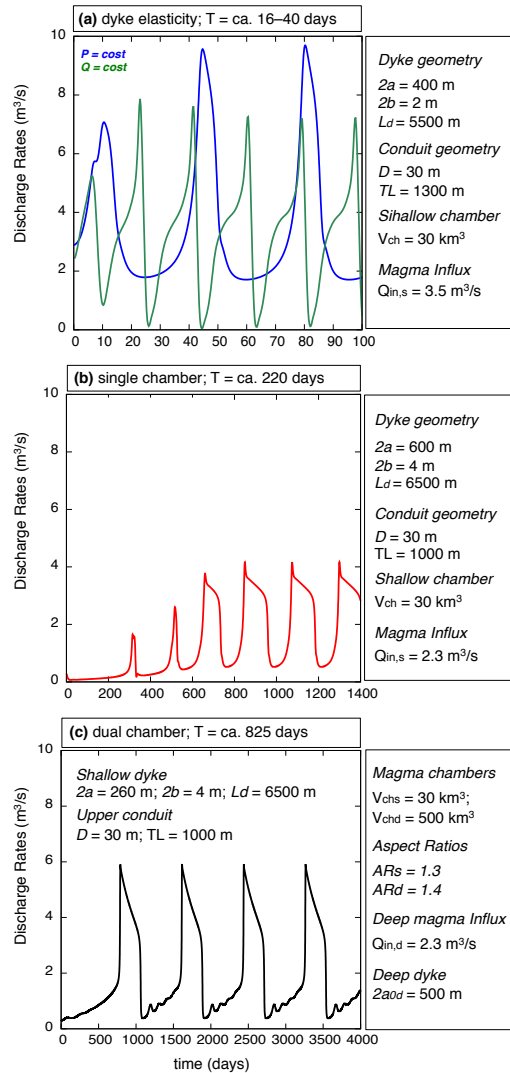
.111

.112

.113



114 Fig. 4



115

116

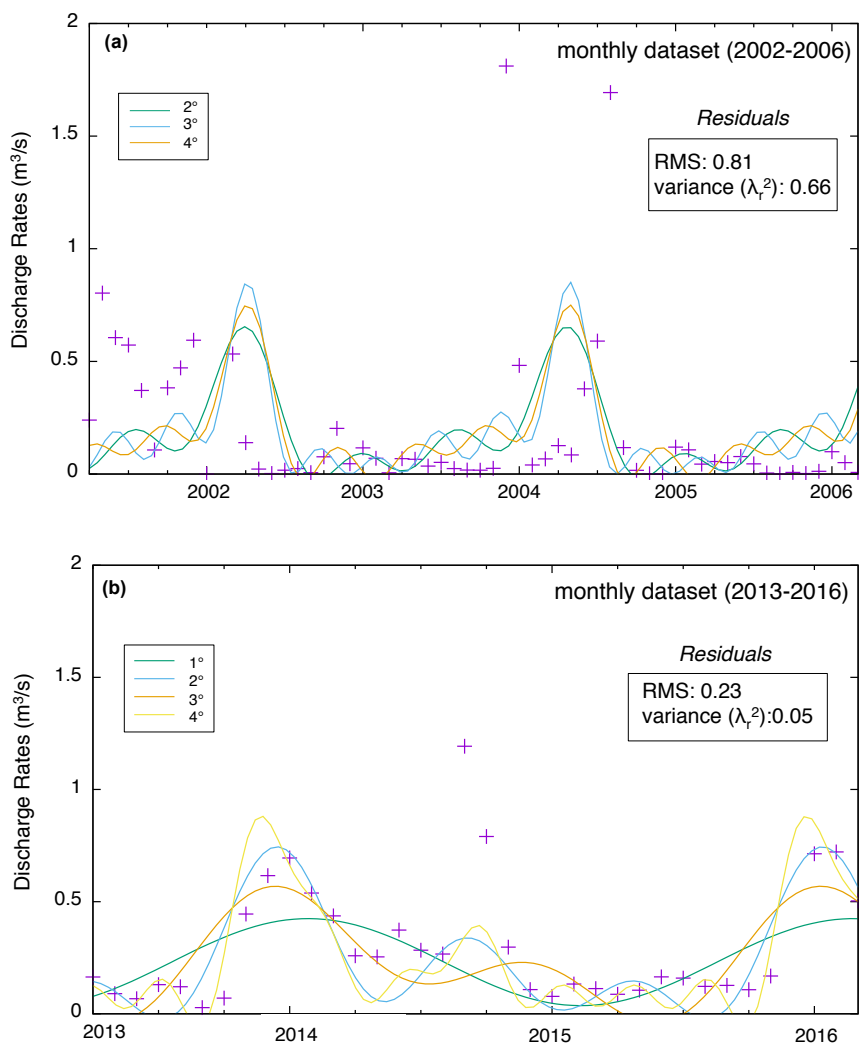
117

118

119



.120 Appendix A1

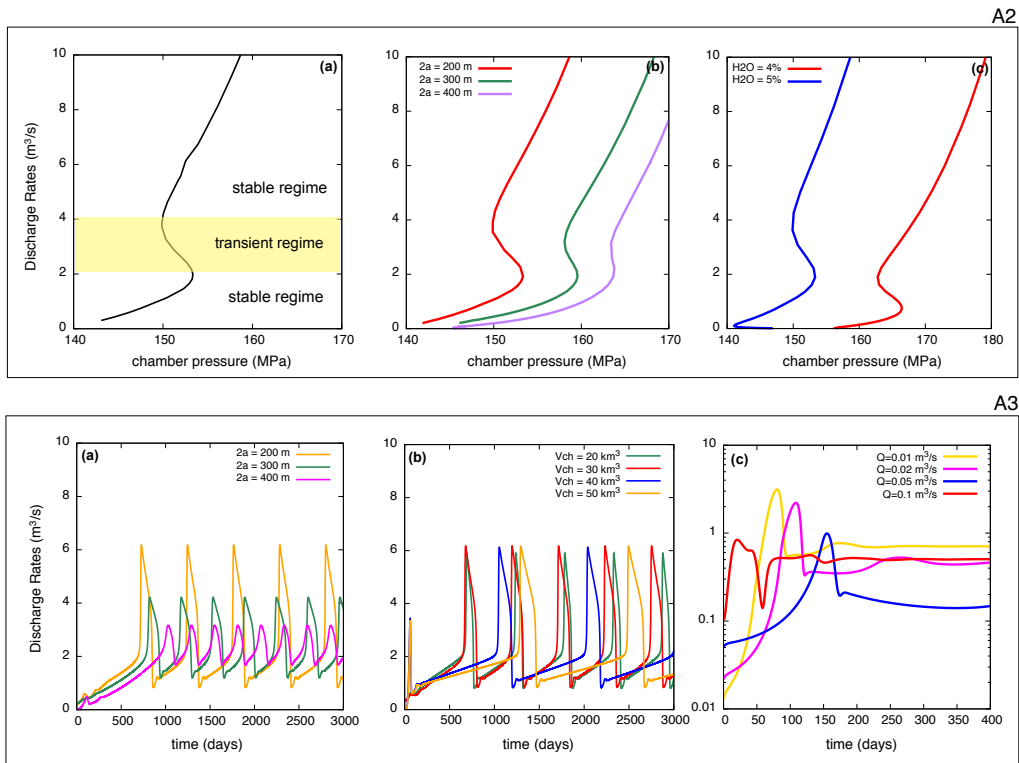


.121

.122



123 Appendix A2 – A3



124

125

126

127

128

129

130

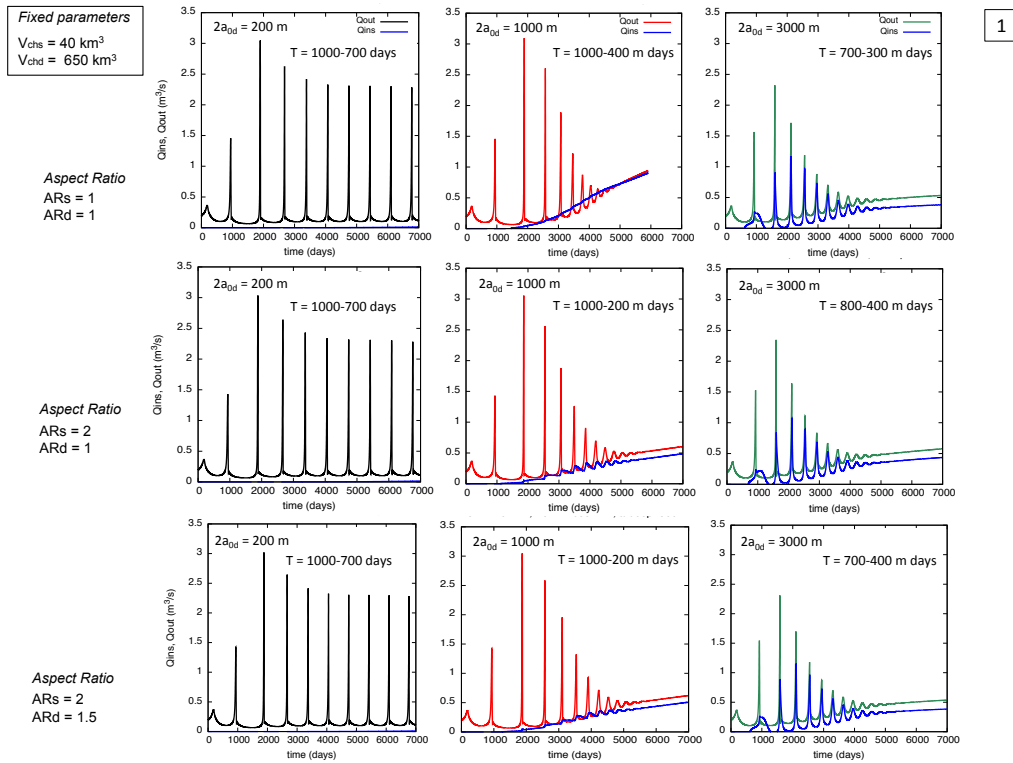
131

132

133



134 Appendix A4



135

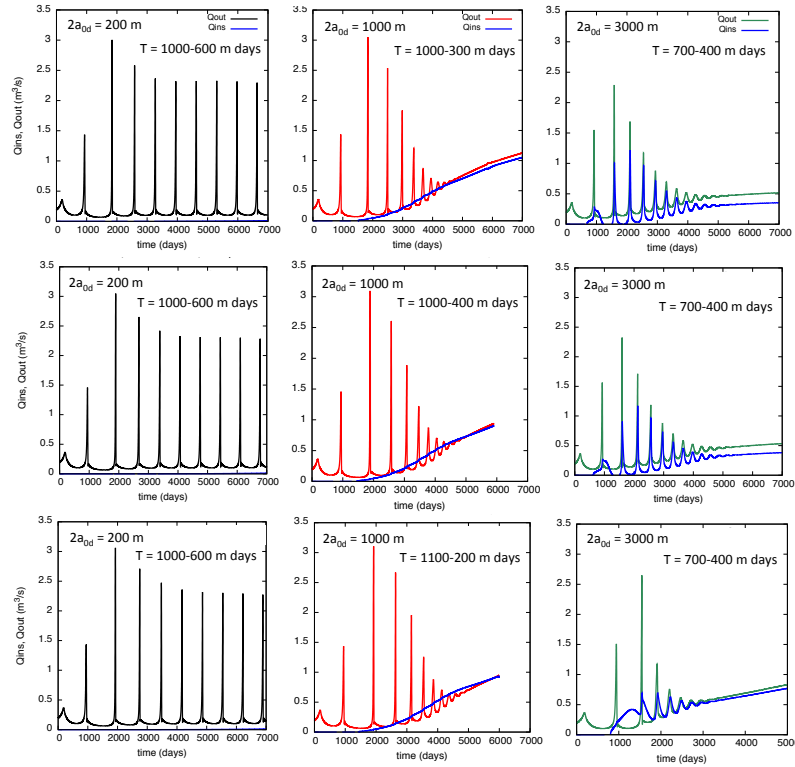


Fixed parameters
 ARs = 1
 ARd = 1
 $V_{\text{chd}} = 650 \text{ km}^3$

Shallow Chamber Volume
 $V_{\text{chs}} = 30 \text{ km}^3$

Shallow Chamber Volume
 $V_{\text{chs}} = 40 \text{ km}^3$

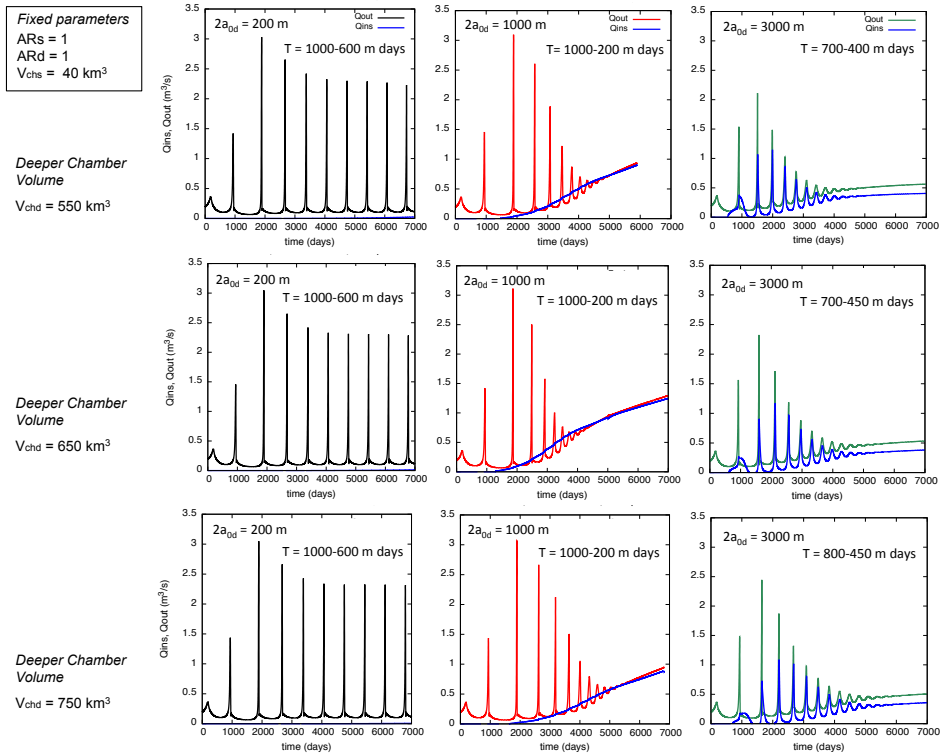
Shallow Chamber Volume
 $V_{\text{chs}} = 50 \text{ km}^3$



2



3



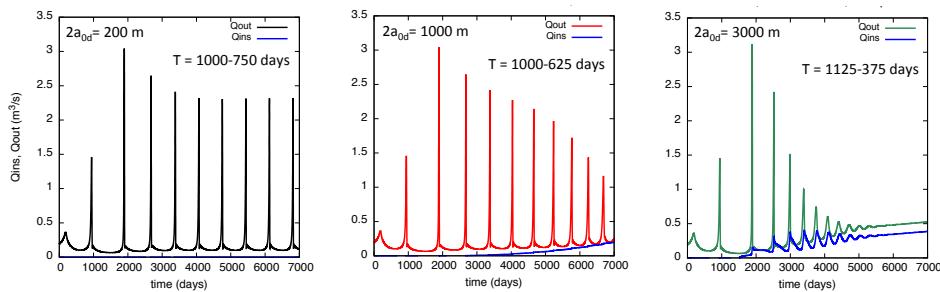
137



Fixed parameters : $ARs = 1$; $ARd = 1$; $Vchd = 650 \text{ km}^3$; $Vchs = 40 \text{ km}^3$

4

▪ $Qin_depth = 1 \text{ m}^3/s$



▪ $Qin_depth = 3 \text{ m}^3/s$

